Third DELTA User-meeting

Dortmund
28. November 2007

Dear reader,

Historically seen are users of synchrotron radiation parasites. They started at large accelerators constructed for atomic physics and used e.g. for high energy collision experiments applying the high brilliant radiation emerging from those machines. The advantages of the radiation are nowadays well known. Synchrotrons especially constructed to produce the radiation to be applied in a variety of experiments in a broad field of applications are available today. An increasing number of parasites larvae mutated from this early stadium to brilliant scientists during time. We have today no more reason to belong to the species of parasitic users. We are a modern family and an innovative community.

The results obtained in 2007 by a small sub-group, The DELTA Users, of this community presented in the third period of report are contained in this book of abstracts and are a vivid proof of it.

Further, we are optimistic looking forward the outstanding mission of education of DELTA recognized and supported by the University of Dortmund. We acknowledge the effort to reoccupy the vacancy of the professorship produced after the retirement of Prof. Wille.

Glückauf.

Alex von Bohlen

DELTA user-meeting 2006

Third DELTA User-meeting

28. November 2007

Agenda

8:50 - 9:10	**Welcome coffee**
9:10 - 9:15	**Opening** *A. von Bohlen and M. Tolan*
9:15 - 9:30	**Hydrate formation in the system CO_2-water: high energy x-ray scattering** *F. Lehmkühler, M. Paulus, C. Sternemann, D. Lietz, and M. Tolan*
9:30 - 9:45	**X-ray investigations for determining the aspect ratio in CdSe nanorods** *Ö. Kurtulus, Th. Fröhlich, Z. Li, A. Mews, U. Pietsch*
9:45 - 10:00	**X-ray reflectivity investigations of $[Co_{60}Fe_{20}B_{20}/MgO]_n$ multilayers** *M. Vadalá, A. Nefedov, G. Nowak, K. Westerholt, and H. Zabel*
10:00 - 10:15	**Lysozyme adsorption at the silica/water interface: an in-situ high energy x-ray reflectivity study** *F. Evers, K. Shokuie, M. Paulus, C. Sternemann, and M. Tolan*
10:15 - 10:45	**Coffee break**
10:45 - 11:00	**Protein-protein interactions revealed by synchrotron small-angle x-ray scattering** *N. Javid, C. Krywka, M. Tolan, and R. Winter*
11:00 - 11:15	**Solution SAXS – proteins under extreme conditions** *C. Krywka, R. Winter, and M. Tolan*
11:15 - 11:30	**XSW measurements of ion distributions above a charged surface** *M. Brücher, A. von Bohlen, C. Sternemann, M. Paulus, and R. Hergenröder*
11:30 - 11:45	**Depth resolved photoemission experiments with soft x-ray standing waves on multilayer systems** *S. Döring, D. Weier, F. Lehmkühler, U. Berges, F. Salmassi, C. S. Fadley and C. Westphal*
11:45 - 13:00	**Lunch break**
13:00 - 13:15	**Photoelectron spectroscopy studies on the system zirconium oxide on Si(100)** *F. Schönbohm, C. Flüchter, D. Weier, M. Schürmann, U. Berges, and C. Westphal*
13:15 - 13:30	**The influence of tetragonal distortion on the electronic band structure of bcc Co(001) and the bcc Co/MgO (001) interface** *F. Matthes, M. Müller, M. Ležaić, L. Plucinski, S. Cramm, and C. M. Schneider*
13:30 - 13:45	**The materials science beamline BL8: progress and first user experiments** *D. Lützenkirchen-Hecht, R. Wagner, and R. Frahm*
13:45 - 14:00	**Structural characterization of Co/Cr/Fe spin-valve systems** *F. Brüssing, G. Nowak, K. Theis-Bröhl, and H. Zabel*
14:00 - 14:15	**Development of a portable wide-energy range micro-focus XRF spectrometer for analysis of aerosol particles from the South Pole** *M. Krämer, S. Maeo, K. Kuzushita, and K. Taniguchi*
14:15 - 14:30	**Coffee break**
14:30 - 15:00	**Discussion on user demands**
15:00	**End of the meeting**

Beamline overview:

BL2
- ISAS Dortmund
- White beam excitation at DELTA bending magnet (critical energy of 2.2 keV)
- Energy and wavelength dispersive x-ray fluorescence spectroscopy

BL5
- Forschungszentrum Jülich
- U250 electromagnetic undulator
- Energy range: 5 - 400 eV
- Photoemission, coincidence measurements, spectroscopy

BL8
- Universität Wuppertal
- Superconducting asymmetric wiggler (SAW) with a critical energy of 7.9 keV
- Energy range: 1 - 30 keV
- Focus on material science
- EXAFS, QEXAFS, ReflEXAFS, x-ray diffraction

BL9
- Technische Universität Dortmund
- Superconducting asymmetric wiggler (SAW) with a critical energy of 7.9 keV
- Energy range: 4 - 30 keV
- X-ray reflectivity, x-ray diffraction, SAXS, XSW, inelastic x-ray scattering

BL11
- Technische Universität Dortmund
- U55 permanent magnet undulator
- Energy range: 55-1500 eV
- Photoemission spectroscopy, photoelectron diffraction

The influence of tetragonal distortion on the electronic band structure of bcc Co(001) and the bcc Co/MgO (001) interface

Frank Matthes[1], Martina Müller[1], Marjana Ležaić[2], Lukasz Plucinski[1], Stefan Cramm[1], and Claus M. Schneider[1]

Institute of Solid State Research
[1]IFF-9 "Electronic Properties"
[2]IFF-1 "Quantum Theory of Materials",
Research Centre Jülich, 52425 Jülich, Germany

Contact: F.Matthes@fz-juelich.de

Motivation

The bcc Co/MgO (001) interface has moved into the focus of recent research activities on magnetic tunneling junctions (MTJ). Theoretical predictions by Zhang and Butler resulted in an enhanced tunneling magnetoresistance (TMR) ratio for the single-crystalline bcc Co/Mgo/Co along the Δ-direction, when compared to the situation in Fe/MgO/Fe [X 1]. The enhancement is ascribed to a total reflection of all electronic wave functions participating in the tunneling process at the counter electrode when the two magnetic Co electrodes are aligned antiparallel. Yuasa and co-workers could demonstrate for a fully epitaxial Co/MgO/Co MTJ a TMR ratio of 410% at room temperature [X 2]. The transport calculations assumed a bcc crystal structure for Co with a lattice constant of a= 2.82 Å and took into account only the bulk electronic band structure. These assumptions may not be valid for arbitrary bcc Co-based tunneling junctions, because bcc-Co is known to be metastable. The bcc crystal structure has to be stabilized by the underlying substrate. Indeed, energetically it is easily possible to introduce a tetragonal distortion in the bcc Co crystal structure [X 3]. Our spin-resolved photoemission studies [1] on the Co/MgO interface already give indications that the experimental data cannot be fully interpreted within the picture of a bcc-Co crystal structure.

Experimental Setup

All experiments have been performed under ultrahigh vacuum conditions (base pressure $1*10^{-10}$ mbar). Co samples of different thickness have been prepared on a 27 ML thick Fe seed layer. As substrates we used GaAs(100) wafer. The crystalline structure of the Co films was monitored by low electron energy diffraction. Above a thickness of about 16 ML the LEED spots fade away due to the onset of the strain-induced lattice transformation into the hcp phase. A detailed description of the substrate preparation and film growth conditions can be found in the PhD thesis of M. Müller [2]. The MgO films were grown by electron-assisted evaporation of Mg in a partial pressure of about $1*10^{-8}$ mbar molecular oxygen.

Spin resolved photoemission experiments

A comparison with a calculated bulk bcc Co electronic structure reveals that the transitions labelled in fig. 1(a, b) cannot be fully assigned, in particular, the minority spin transition **B** remains unaccounted for [2]. In the framework of a bulk band structure picture peak **B** is a result of a tetragonal compression of the crystal along the c axis. As a consequence of the lattice deformation the above mentioned Δ_1 minority state located above the Fermi level will

be pushed below the Fermi energy. This may have severe consequences for the electronic transport properties of bcc Co based MTJs, because the total reflection of the Δ_1 electron wave function – which represents the largest conductivity channel – will now be lifted. This should result in a strong decrease for the resulting TMR ratio.

In addition to the bulk band structure, we have to evaluate the influence of possible surface states. In the case of bcc Fe(001), a minority surface state exists at the Γ point 0.2 eV above the Fermi level. In a cooperation with our theory department, the effect of a tetragonal distortion along the [001] direction upon a bcc Co surface was modelled. Performed semi infinite KKR calculations based on LDA confirmed the tetragonal distortion induced shift of the bulk minority Δ_1 state below the Fermi level. In addition, a minority Δ_1 surface state located at the Fermi level was predicted, whose binding energy matches the position of transition **B** (fig. 1a-b).

Our experimental photoemission data (fig. 1c) show that the peak related to the surface state for the uncovered Co surface still persists after the coverage with an MgO layer. The question arose whether the surface state is converted into an interface state or whether the shifted minority Δ_1 bulk state induced by tetragonal distortion, is responsible for transition **B**. Slab calculations of a 5 ML MgO/ 11 ML Co super cell confirmed that the interface state is shifted above the Fermi level. As this method assumes a periodic arrangement of the super cell, we still have to perform semi infinite calculations to exclude the existence of quantum well states evoked by the periodic boundary conditions.

A comparison of the spin-resolved photoemission spectra (fig. 1a-b) for a 6 and 12 ML thick film yielded a further detail deviating from bulk band structure model: a broadening in binding energy for transition C (related to bulk majority Δ_5 state). Results of semi infinite KKR calculations give indications that this experimental finding is related to a hybridisation with the underlying iron seed layer.

The presented spin-polarized valence band photoemission spectroscopy experiments provide a better understanding of the electronic interface structure for the tetragonal distorted Co/MgO system. In particular, a fruitful cooperation between theory and spin-resolved photoemission spectroscopy offers a possibility to design the electronic interface conditions with the aim to improve spin-dependent electronic transport properties in future spintronic devices.

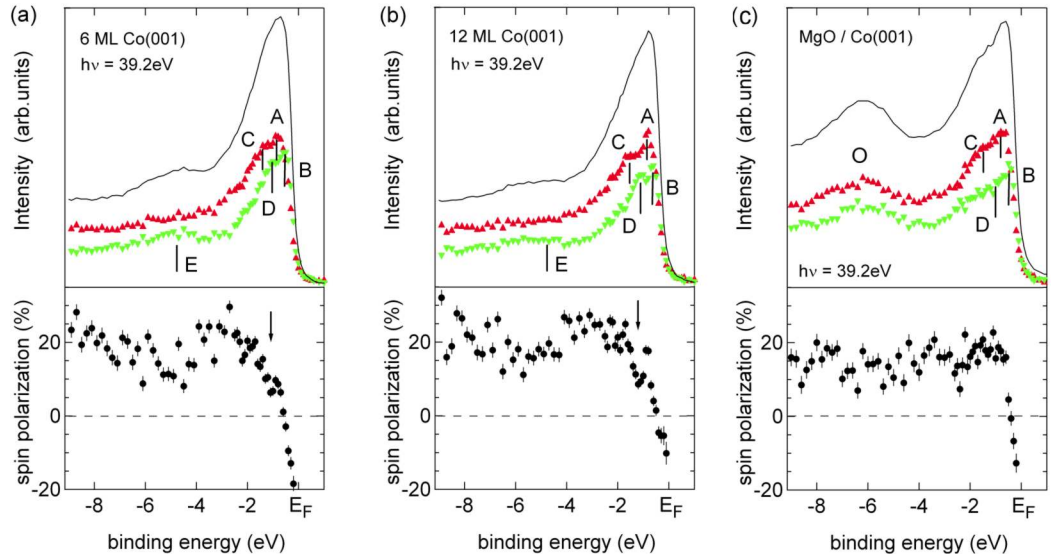

Fig 1. Spin-resolved photoemission spectra, normal emission, p-polarized light incident under 45° with respect to the sample normal. Solid line denotes spin integrated data, red triangles represent majority spin electrons, green triangles minority spin electrons.

Topic related publications

[1] L.-N. Tong, C.-L Deng, F. Matthes, M. Müller, C.M. Schneider, C.-G. Lee,"Influence of MgO overlayers on the electronic states of bct Co(001) thin films grown on bcc Fe(001)/GaAs(001)", PRB 73(2006) 214401

[2] Dissertation Martina Müller, Electronic Structure of Ferromagnet-Insulator Interfaces: Fe/MgO and Co/MgO, 2007, Schriften des Forschungszentrum Jülich, Reihe Materie und Material, Band 40, ISBN 978-3-89336-493-0

[3] Martina Müller, Frank Matthes, Claus M. Schneider, "Spin polarization at ferromagnet-insulator interfaces: The important role of stoichiometry in MgO/Fe(001)", European Physics Letters **80** (2007), 17007

References:

[X 1] X.-G. Zhang and W. H. Butler, Phys. Rev. B **70** (2004)

[X 2] S. Yuasa, X.-G. A. Fukushima, H. Kubota, Y. Suzuki, and K. Ando, Appl. Phys. Lett. **89** (2006) 042505

[X 3] S. Fox and H.J.F. Jansen, Phys. Rev. B **60** (1999), 4397

Progress at the Materials Science Beamline 8 at DELTA

D. Lützenkirchen-Hecht, R. Wagner, U. Haake and R. Frahm

Fachbereich C – Physik, Bergische Universität Wuppertal,
Gaußstr. 20, 42097 Wuppertal, Germany

In this contribution we report on the progress made at the wiggler Beamline 8 at the DELTA storage ring and the improvement of the hard- and software during the past period. The characterization of the Si(111) optics was subject of previous studies in the photon energy range from about 7 to 12 keV [1], yielding i.e. an improved energy resolution compared to well established EXAFS-beamlines such as RÖMO 2 at HASYLAB [2]. The application of the Si(311) optics for EXAFS experiments at higher energies above about 20 keV was systematically investigated and the focussing properties of the crystal bender was studied in detail. Using this optics, first high energy EXAFS spectra were collected in transmission mode. As examples spectra obtained from a Mo-metal foil at the Mo K-edge at 20 keV as well as a Pd K-edge spectrum (24.35 keV) of a $PdCl_2$ powder sample are presented in Fig.1. The data quality at the Mo K-edge is excellent with clear fine structure oscillations up to 18 $Å^{-1}$, corresponding to a photon energy of about 1300 eV above the edge. The data acquisition at the Pd K-edge is more difficult due to the rapidly decreasing photon flux provided by the superconducting asymmetric wiggler for those X-ray energies, which are more than three times higher than the critical energy of 7.9 keV. Additional measurements have shown that XANES experiments are still feasible for energies higher than ca. 28 keV, however, certain limitations apply for EXAFS experiments for energies above ca. 23 keV.

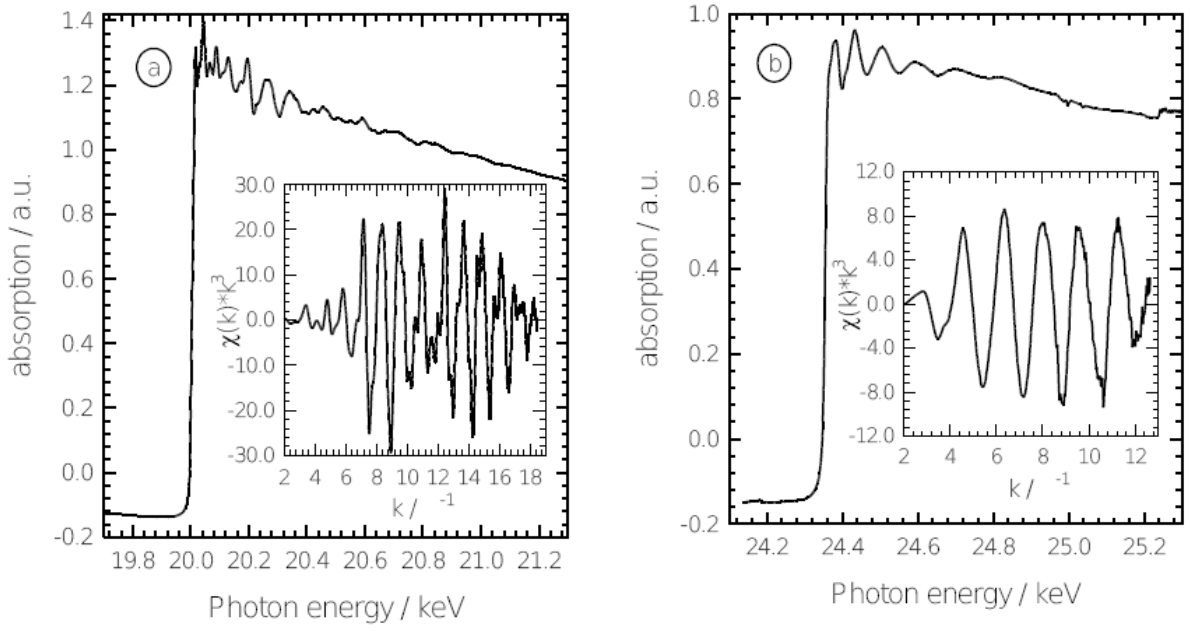

Fig. 1: (a) Transmission mode EXAFS spectra of a Mo metal foil at the Mo K-edge (20.0 keV) and (b) of a $PdCl_2$ powder sample at the Pd K-edge (24.35 keV).

While transmission mode data acquisition is in general well suited for the investigation of bulk materials, thin films and surface structures can only be probed by grazing incidence X-ray absorption spectroscopy (see e.g. [3-5]). In this context, we have recently measured the first (ex-situ) reflection mode EXAFS of sputtered thin metal films under total reflection conditions at BL 8. For the experiments presented here the Si(111) monochromator was used.

A slit system in front of the sample defined the shape of the impinging beam and a second slit system was used in front of the second detector for the measurement of the reflected intensity. The angular positioning of the samples and the detectors (Ar filled ionization chambers) was done using the multi-purpose diffractometer at the end of the beamline. For the first experiments, sputtered gold films have been investigated in the vicinity of the Au L_3-edge (11.919 keV). A typical example is presented in Fig. 2 for a film of ca. 58 nm thickness together with a reflectivity profile shown in the insert. The data quality obtained is excellent, thus in-situ studies - especially of reactive sputtering processes [5, 6] - are planned at BL 8 in the near future.

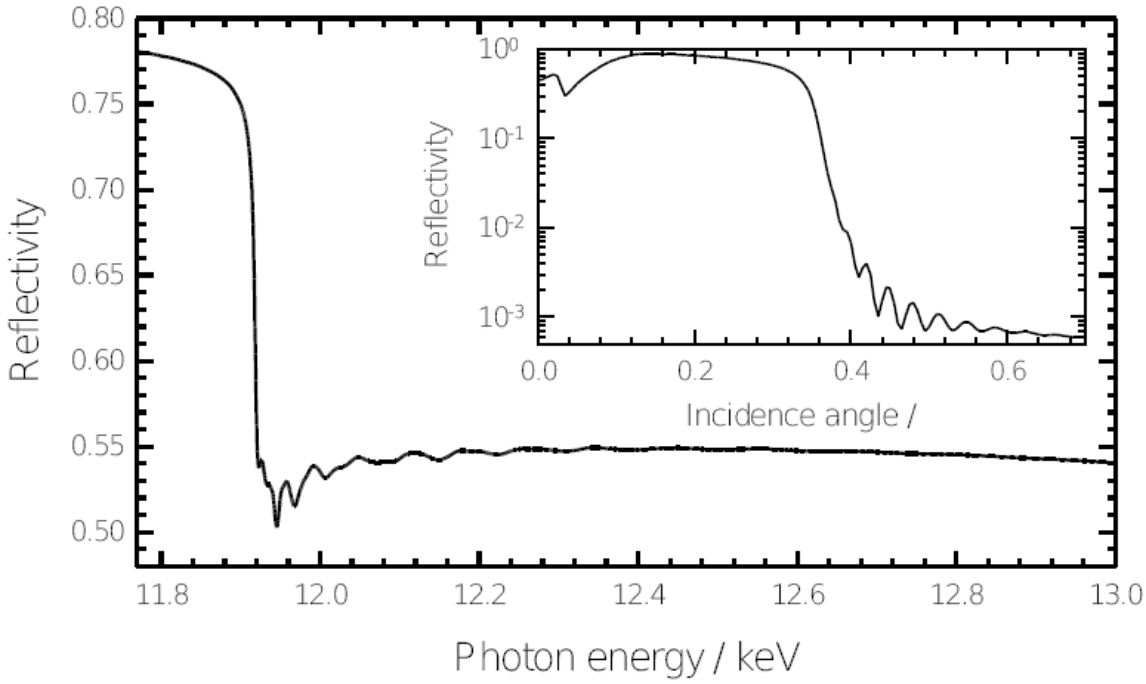

Fig. 2: Reflectivity EXAFS spectrum of a sputtered Au film (thickness ≈ 58 nm) at the Au L_3-edge for an incidence angle $\phi = 0.3°$. In the insert, the specular reflectivity profile is shown for a photon energy E = 11.6 keV. The typical reflectivity oscillations are clearly visible above the critical angle.

References:

[1] A. Watenphul, Diploma Thesis, University of Wuppertal (2006)
[2] R. Frahm, Rev. Sci. Instrum. 60 (1989) 2515
[3] D. Lützenkirchen-Hecht, M. Wagemaker, et al., Surf. Sci. 538 (2003) 10
[4] D. Lützenkirchen-Hecht, R. Frahm, Physica B 357 (2005) 213
[5] D. Lützenkirchen-Hecht, R. Frahm, Surf. Sci. 600 (2006) 4380
[6] D. Lützenkirchen-Hecht, K. Bruder, et al., Rev. Sci. Instrum. 76 (2005) 073905

Beamline 8 at DELTA: First user experiments

D. Lützenkirchen-Hecht[a], R. Wagner[a], S. Cammelli[b], C. A. Degueldre[b], B. Arezki[c], U. Pietsch[c], R. Frahm[a]

a) Fachbereich C – Physik, Bergische Universität Wuppertal, Gaußstr. 20, 42097 Wuppertal, Germany
b) Paul Scherrer Institut, CH-5232 Villigen PSI , Switzerland
c) Faculty of Physics - Department of Solid State Physics, Universität Siegen, Walter-Flex-Straße 3, 57072 Siegen, Germany

During the last few month, the first user experiments were performed at beamline 8 at the DELTA storage ring, on which we want to give a brief overview in this contribution. On of the conducted experiments concentrates on steel materials that are employed in nuclear reactor pressure vessels (RPV) which are composed by an iron base alloy with traces of Ni and Cu (and additional elements) in the 0.1-1 wt.% range. The most important material degradation in RPV-steels during operation in a reactor is the embrittlement caused by the formation of small metal precipitates in the iron matrix. These precipitates, which mainly consist of small Cu and Ni atom clusters, are able to pin dislocations and hinder dislocation gliding, thus leading to a less ductile behaviour. On a macroscopic scale, this modification of the elastic properties of the material lead to a situation where the structural integrity of the reactor pressure vessel in a nuclear power plant can be critically affected. Therefore, significant work has been done in the past in studying RPV steel aging and coupling microstructural information with the mechanical behaviour of such steels.

In the present experiments, we want to investigate the changes of the distribution and the local environment of Cu and Ni in the RPV-steel induced by irradiation with high neutron fluxes and its relaxation by a subsequent annealing. The experiments were performed using Si(111) optics, an ionization chamber for the measurement of the incoming beam, and a Si pin-diode with a multichannel analyzer and digital pulse processor to measure the fluorescence signals excited in the sample. Typical raw data obtained at the Ni K-edge for a sample containing only 0.8 wt% of Ni within about 25 min. of integration time are presented in Fig. 1.

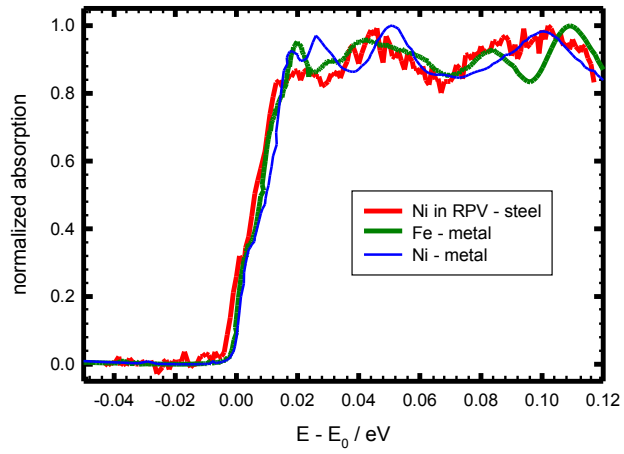

Fig. 1: Near edge fluorescence EXAFS spectrum of a Fe-alloy with 0.8 wt.% Ni at the Ni K-edge (8.333 keV). For comparison, near edge spectra of bulk fcc nickel and bcc iron are also shown on a relative energy scale.

As can be seen, the near edge region of this spectrum is quite different to that of bulk (fcc) nickel, due to the distribution of the Ni-atoms on regular bcc lattice positions within the iron matrix. In contrast, the XANES is more similar compared to bulk (bcc) Fe, and the irradiation of this metastable configuration with neutron causes the creation of vacancies on both Fe and

Ni sites, and a clustering of interstitial Ni to form small fcc-particles in the bcc iron matrix, as will be studied in more detail in the future. In the present case, one big problem for the data analysis is the overlap between the different fluorescence lines resulting from the energy resolution of about 200 eV: While strong Fe K_α and K_β peaks were detected at 6.4 keV and 7.1 keV, only weak contributions from the alloyed Ni could be measured at 7.5 keV and 8.2 keV. These can however be eliminated by a proper peak deconvolution, which is currently under way.

A second user experiment deals with EXAFS investigations of metallo-supramolecular polyelectrolyte-amphiphile-complexes (PACs). PACs are of particular interest because the spin state of metal ions (and thus the magnetization of the system) can be switched by temperature, light or pressure, making these materials an alternative for future applications in molecular memory and switching devices. In a previous work on powdered PACs, it has been shown that the spin transition is irreversible [1]. Is is well known now that the low-spin (LS) to high spin (HS) transition can be initiated by illumination with visible light (LIESST - Light-induced-Excited-Spin-State-Trapping) which has been demonstrated for various molecular systems. It has been also demonstrated by EXAFS that this photo-induced spin transition is associated with a deformation of the octahedral coordination symmetry around the metal cations [2]. Here we want adress that also under the conditions of a supramolecular arrangement LIESST takes place and could be observed (and even switched) by a local deformation of the Fe-N octahedra. At present, it is an open question how the coordination shell of the $Fe2^+$-ions changes after irradiation with light. Using powdered metallo-polyelectrolyte samples containing both Fe and Ni and different amounts of amphiphiles, first transmission mode EXAFS experiments were performed at the K-edges of the envolved metal cations; examples are presented in Fig. 2.

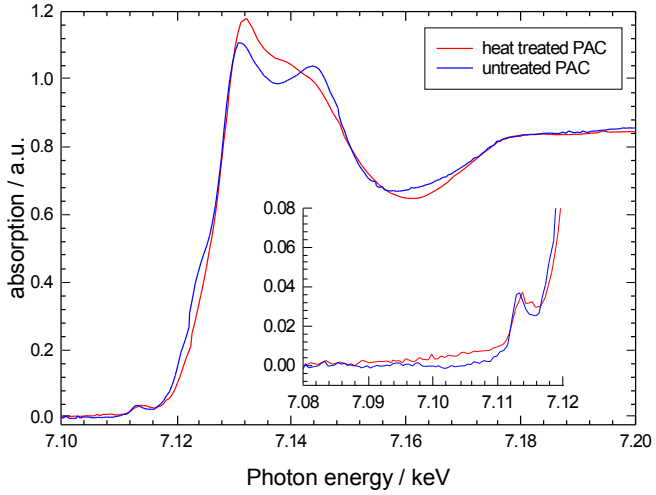

Fig. 2: Near edge spectra of an untreated (low-spin) and a heat-treated (high-spin) PAC with 12 amphiphiles per metal centre at the Fe K-edge. Both the pre-edge peaks (insert) as well as the near-edge structure are significantly different indicating a different degree of deformation of the Fe-N octahedra in both states which is a signature of the LS-HS-transition.

References:

[1] Y. Bodenthin , U.Pietsch, et al. Phys. Rev. B 76 (2007) in print.
[2] H. Oyanagi, T. Tayagaki and K. Tanaka, J. Phys. Chem. Sol. 65 (2004) 1485.

Thickness dependent ordering and orientation of low molecular weight Poly(3-hexylthiophene) OFET layers

Siddharth Joshi[1], Souren Grigorian [1], Ullrich Pietsch[1], Patrick Pingel[2], Achmad Zen[2], and Dieter Neher[2]

[1] Festkörperphysik, Universität Siegen, Siegen, Germany
[2] Institut für Physik, Universität Potsdam, Potsdam, Germany.

The correlation between the surface morphology, crystal structure and the charge-carrier mobility in Poly(3-hexylthiophene) (P3HT) is not well-understood[1]. In order to find a relation between the thickness dependence of structural order and electrical parameters we have performed in-plane and out-of plane X-ray diffraction measurements with synchrotron radiation of thin semi-crystalline films of low molecular weight P3HT prepared by spin coating technique[1,2]. We have investigated samples with film thickness varying between 10-40 nm.

X-ray out-of-plane scans and reflectivity measurements (wavelength λ=1.12 Å) were carried out at beam line BL9 at the Delta Synchrotron Source (DELTA), Dortmund, Germany. Due to the lower flux, in-plane scans were not possible to detect at DELTA, in-plane measurements were performed at European Synchrotron Research Facility (ESRF), Grenoble, at the undulator beam-line ID10B ('Trokia II'), using a wavelength of 0.924 Å.

The diffraction curves as shown in fig. 1(A) & 1(B) can be interpreted by scattering from nano-crystallites with mean size of 25 nm, embedded in an amorphous matrix[3]. The nanocrystallites may have different crystal structures which in average are indexed by a monoclinic unit cell measured in direction parallel to the surface normal and all the diffraction peaks reveal independent from the film thickness. In contrast to this in direction perpendicular the set of peaks related to the lamellar stacking of molecules (100, 200,…) show strongly decreasing intensity for decreasing film thickness but other peaks associated with distance of neighboured thiophene rings (020) and (002) keep unaffected. This is interpreted by a preferential pinning of nanocrystals at the film to substrate interface when the crystal size becomes in the order of the film thickness. X-ray diffraction measurements have been performed between room temperature and about 100°C. For thick films the out-of plane (100) peaks become less intense and shifts to smaller angles with increasing the temperature. At the same time the in-plane (020) peak position increases. With decreasing film thickness the melting temperature of crystallites shows an increase to higher temperatures. The phase transition appears rather continuous for thicker films but becomes sharp for the thinnest films (10 nm). The thickness behaviour of structural parameters correlated well with the thickness dependence of mobility measured at OFET devices. The mobility is found to be constant for thick layers but it drops by one order of magnitude for samples with thickness below 20 nm. This suggests a model of charge transport in low molecular weight P3HT which is realized mainly through nano-crystallites pinned at the film to substrate interface. Whereas for thick layers the charge carrier can find neighboured crystallites in bulk they are scattered at the grain bounders in thin films.

For the first time we have shown that the crystalline order of films made of P3HT changes as function of film thickness. For film thicknesses above 20 nm the film structure consists of nanocrystallites of 25...40 nm size diluted in an amorphous matrix. For films below 20 nm the changes are remarkable: we have found a drop of 100 peak intensity and a change in the temperature dependence of peak position and peak intensity. The disappearance of 100 peaks in GID can be interpreted by a preferential alignment of nanocrystals at the film to substrate interface[4]. Considering the average crystal size the change in alignment appears when the domain size becomes in the order of the film thickness. As crystalline order the mobility

drops at film thicknesses below 20 nm. The crystal structure of nanocrystals could be refined to be monoclinic unit cell.
We found a complete change of crystal unit cell with increasing temperature[4]. Moreover, the phase transition between solid and melt changes as function of temperature.

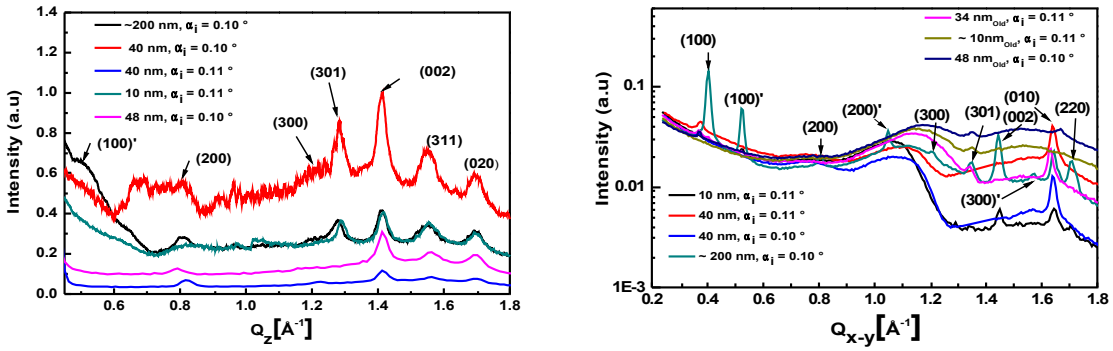

Fig. 1: (A) Fig. 1. Out-of-plane ´thickness dependent scan for low molecular weight fraction of P3HT, (B) thickness dependent in-plane scan of P3HT, low molecular weight fractions for different α_i.

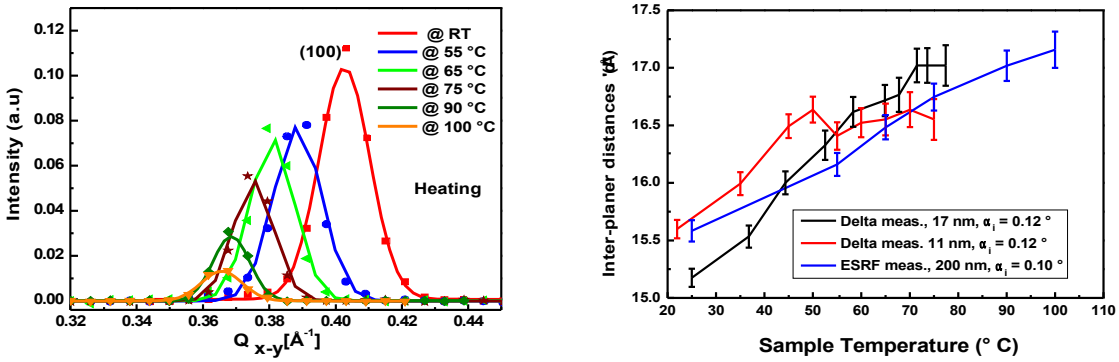

Fig. 2. (A) Relative intensity versus temperature, (B) ‘d’ spacing Vs temperature dependent study of low molecular weight P3HT fractions.

It is found continuous (second order) for thick films but sharp (first order) for thinner films. This gives a rough estimate for the decay length of interface interaction towards the bulk. Because the peaks width remains constant while decreasing in intensity the number of crystallites decrease within creasing temperature for film thickness above the interface decay length. The crystals dissolve and the amorphous film which melts as a whole. This differs from thin films where the crystals keeps pinned at the film-substrate interface up to the melting temperature. Due to the interface interaction the later one is expected to change as function of film thickness. This needs further systematic investigation.

Acknowledgment

We would like to thank all the BL9 beamline staff at Delta synchrotron source, Dortmund, Germany and ID10B beam line staff at the ESRF for their valuable help. This work was financially supported by the DFG under the project of emphasis: SPP 1121.

References:

1. A. Zen et al., Macromolecules, 39 (2006) 2162.
2. R. J. Kline et al., Nature materials, 5 (2006) 222.
3. A. Zen et al., Adv. Funct. Mater. 14 (2004) 757.
4. S. Joshi et al. physica status solidi a, submitted

High Resolution Measurement of the Thermal Expansion Coefficient of Semiconductor Multilayer Lateral Nanostructures

B. Brüser, T. Panzner, S. Grigorian, J. Grenzer, U. Zeimer and U. Pietsch

The aim of our experiment is to measure the thermal expansion coefficient of a pure semiconductor multilayer before and after preparation of a lateral nanostructure. In this experiment our nanostructure sample consists of a multilayer system with 5 periods of an InGaAs/GaAs multi-quantum-well grown on [001] a GaAs substrate. The Indium concentration amounts to 22 %. The surface nanostructure of the sample was prepared via holographic exposure and subsequent wet chemical etching with a lateral periodicity of 300 nm. The sample has a total superlattice thickness of 54,7 nm.

The samples were measured at DELTA´s BL9. The samples were mounted onto an evacuated heating stage (Anton-Paar DHS 900). We used coplanar x-ray diffraction in order to measure the rocking curves (ω/2θ-scan) of the symmetric 004 reflection. Our scan direction corresponds to a longitudinal scan, i.e. it will show the oscillations of the superlattice but not the grating peaks. The curves were recorded at two different temperatures, i.e. at 17°C and at 400°C. Considering the smallness of the expected effect we used an analyzer crystal (Ga-004) in front of a scintillation counter. Our beamsize was 1mm² and the energy was set to 8 keV.

First, we measured the region of the non patterened area of the sample followed by measurement for the patterned part of the sample. Two typical diffraction curves of the non-patterned sample area are shown in Fig.1.

Both curves show distinct superlattice peaks in addition to the Bragg peak of the GaAs substrate. The angular distance between the superlattice peaks are inversely proportional to the thickness superlattice period. Due to thermal expansion this angular distance is supposed to change at different temperatures, i.e. the thermal expansion coefficient of the superlattice can be measured from the change of the angular distance between the superlattice peaks.

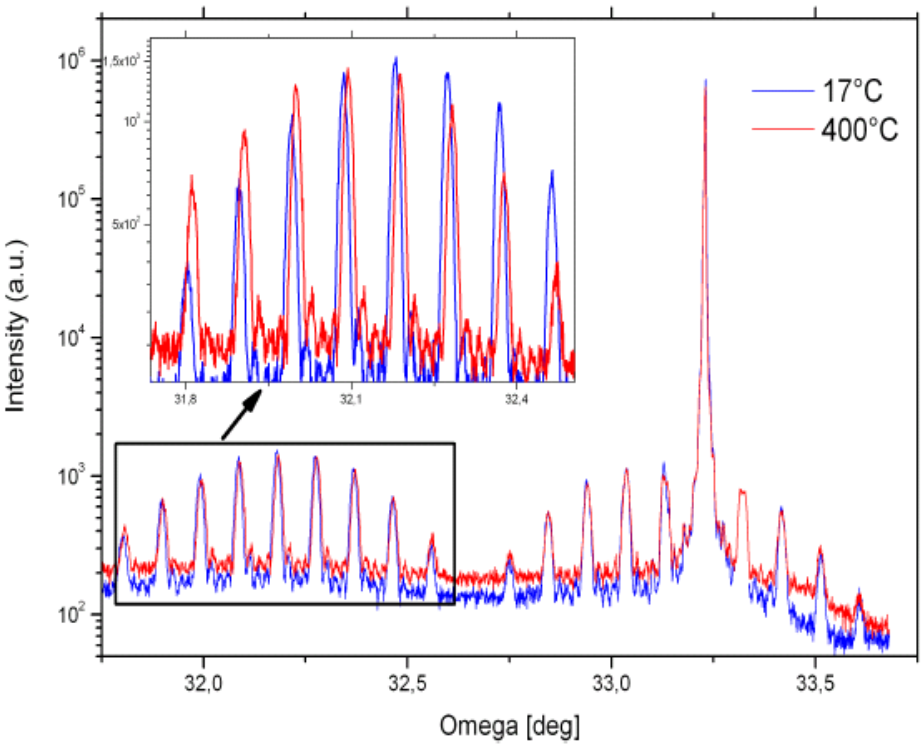

Figure 1: 004 Reflection at two different temperatures (ω/2θ-scan) revealing the superlattice structure

From previous measurements the thermal expansion coefficient of the bulk material (GaAs) has been determined. It amounts to $\alpha_{Substrate}$=6,4 10^{-6} K^{-1}. Since the multilayer has been grown pseudomorphically onto the substrate the unit cell is tetragonally strained. Previous work shows an increase of the TEC of up to 40% compared to the non-strained materials due to the tetragonal deformation [1].

Table 1: Experimentally and theoretically determined values for the out-of-plane TEC of the SL sample with and without surface grating. [2]

Surface Structure	TEC(exp.) [$10^{-6}K^{-1}$]	TEC(theor.) [$10^{-6}K^{-1}$]
Gratings	9.8 ± 3.8	7.6
Planar	12.3 ± 2.3	12.0

Evaluation of the data recorded at DELTA shows that the thermal expansion coefficient of the patterned and non-patterned multilayer systems are different (Table1).

The origin of this difference can be explained by a strain field reduction in the samples' top layer implicated by the lateral patterning. This explanation is supported by FEM simulations [2].

Acknowledgements

We thank the Beamline staff at BL9 for their support.

References:

[1] J. Bak-Misiuk, J. Wolf, U. Pietsch, phys. stat. sol. (a) **118,** 209 (1990).

[2] B. Brüser et. al., phys, stat.sol. (a), submitted.

X-ray investigations for determining the aspect ratio in CdSe nanorods

Özgül Kurtulus and Ullrich Pietsch

Fachbereich Physik, Festkörperphysik, Universität Siegen

Semiconductor based 1D nanostructures are of high technological interest due to potential application in 1D conductivity measurements and optical devices. Catalyst assisted solution-liquid-solid synthesis is a new method where nanocrystal catalysts are used to grow CdSe nanowires (NW) from solution. The aim of this study is to investigate CdSe samples prepared with this new method by means of x-ray diffraction. The measurements were performed at BL10 and BL9 beamlines at DELTA using a beam of wavelength 1.127Å. It is found that the CdSe NWs have a crystal structure of wurtzite with an aspect ratio changing between 2 and 10.

The preparation of nanorods and nanowires (NW) with modulated compositions and new methods has led to many scientific developments. The previous methods used could not be applied successfully to synthesize cadmium chalcogenide NWs with diameters that exhibit quantum confinement effects [1]. Catalyst assisted solution-liquid-solid synthesis is a new method where nanocrystal catalysts are used to grow CdSe NW from solution. Here, Bi nanocrystal catalysts which are bound in carbon nanotubes are loaded into a flask with a solution containing Cd/TDPA as reactive precursor. After heating the flask up to 330°C, a drop of TOPO-Se is injected onto the substrate resulting in CdSe NWs grown in a direction perpendicular to the carbon nanotube. The samples were deposited in a glass capillary providing random orientation of NWs with respect to the capillary length axis. Inspection by TEM have revealed that the length of these NWs can be large as few microns. Therefore, this kind of preparation technique is very challenging for application of 1D conductivity.
The measurements have been performed at DELTA synchrotron using a beam of wavelength 1.127 Å. After test measurements at BL10 using a point detector, an image plate system equipped in three different distances from sample at BL9 was used successfully. Fig. 1 shows a 2-dimensional picture of x-ray diffraction measurement. The powder diffraction curves of NW fractions with different Bi nanocrystal concentrations are seen in Fig. 2. The peak positions can be interpreted by crystal structure of wurtzite. It is clearly seen that the 002 peak is sharper than 100 and other directions oblique with respect to the wurzite c-axis which is in accordance with previous works [2, 3]. In Fig. 3, the diffraction curves of NW fractions with different acids in TOPO solution are observed and it is showing a similar behaviour. After correction by apparatus width, the crystalline sample extensions, D_{002} and D_{100}, are determined along and perpendicular to the c-axis using Scherer equation; $D = \lambda / \Delta\theta \cos\theta$

It is always found an aspect ratio (which is simply the length-to-width ratio) of D_{002} / D_{100} = 2…10, only. Presently our finding is interpreted by the appearance of stacking faults which separate the uniformly stacked AB, AB layers from each other.
The experiments with samples prepared at different conditions are going on by x-ray investigations. During these studies, it is planned to concentrate on a nanosized part of the crystal. The results obtained would be helpful for the development of CdSe NWs with self-organized liquid crystals.

We would like to thank all the BL9 and BL10 beamline staff at DELTA for their help during the measurements.

Fig. 1. 2 dimensional picture of x-ray diffraction from CdSe NW

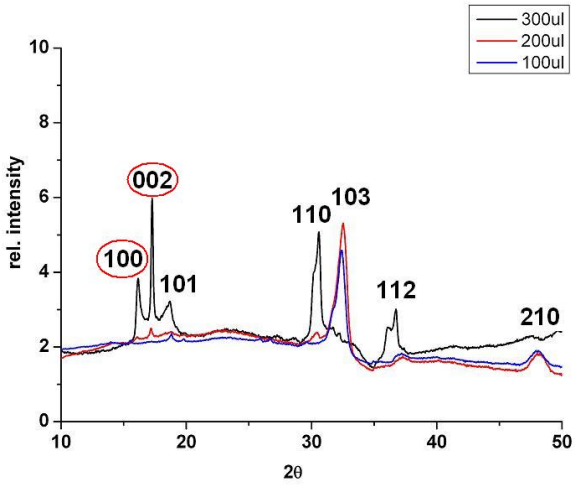

Fig. 2. Powder diffraction curves of NW fractions with different Bi nanocrystal concentrations

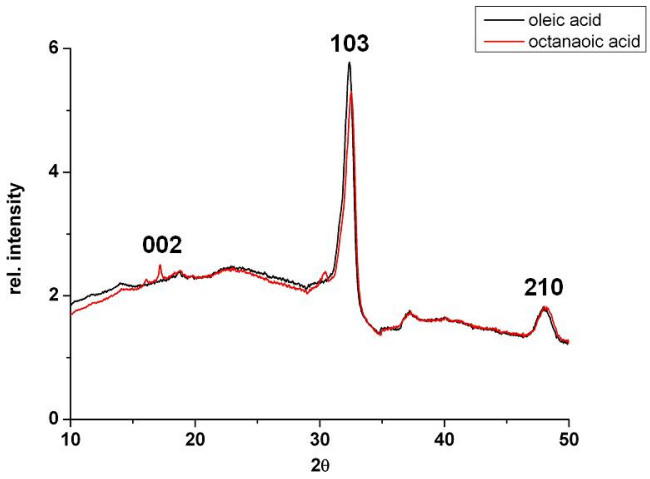

Fig. 3. Powder diffraction curves of NW fractions with different acids in TOPO solution

References:

5. F.Wang, et al., Inorg. Chem., **45**, 7511 (2006).
6. L.Ouyang, et al., J. Am. Chem. Soc., **129**, 133 (2007).
7. S.D. Bunge, et al., Journal of Materials Chemistry, **13**, 1705 (2003).

X-ray Diffraction study of the crystallographic structure and orientation of Metal-Organic Frameworks (MOFs) grown on Functionalized Organic Surfaces

Osama Shekhah, Hui Wang and Christof Wöll

Ruhr-Universität Bochum, Lehrstuhl für Physikalische Chemie 1, 44780 Bochum, Germany.
woell@pc.rub.de

A novel approach for the synthesis and growth of Metal-Organic Open Frameworks (MOFs) based on organic ligands (OL) like benzenetricarboxylic acid (BTC) and inorganic connecters, metal ions (ML)(like Zn(II) and Cu(II)) on an appropriately functionalized organic surface prepared by self assembly of organothiols on Au, has been developed in our group [1]. The approach is based on the sequential immersion of the SAM (self assembled monolayer) covered substrate separately in both of the ML and OL solutions.
The growth of the MOFs was characterized using different techniques like XPS, IRRAS, NEXAFS, SEM, AFM and XRD (using both a laboratory (Cu Kα) as well as a synchrotron radiation source (DELTA, Dortmund). The IRRAS results in addition to XPS results showed a linear increase in the thickness of grown layers per immersion cycle. The AFM and SEM data demonstrated the selective deposition of the grown MOFs layers on the COOH terminated SAMs. The NEXAFS and the IRRAS data provided information about the orientation of the BTC-units, which was mainly perpendicular to the surface in case of Zn(II)-BTC MOFs, yielding a structure of almost vertical layers of the authentic Zn(II)-BTC MOFs which are interconnected – as in the bulk structure - by water-molecules. Attempts to obtain a powder XRD pattern for MOFs with thickness of up to 8 layers were unsuccessful.
In the case of Cu(II)-BTC, we were able to obtain high-quality XRD data, both for out-of-plane and in-plane conditions. The experiments were carried out using a laboratory (Cu Kα) as well as a synchrotron radiation source (DELTA, Dortmund). A typical diffraction scan for a 40 layers Cu^{2+}/BTC multilayer is shown in Figure 1. This out-of-plane diffraction scan clearly demonstrates the presence of a highly ordered and preferentially oriented crystalline material with a periodicity of 6.5 Å normal to the surface. Together with the in-plane data (see Figure 1, inset) this demonstrates unambiguously that the deposited multilayer exhibits the same structure as observed for the bulk compound $[Cu_3BTC_2(H_2O)_n]$ [2].

Fig.1

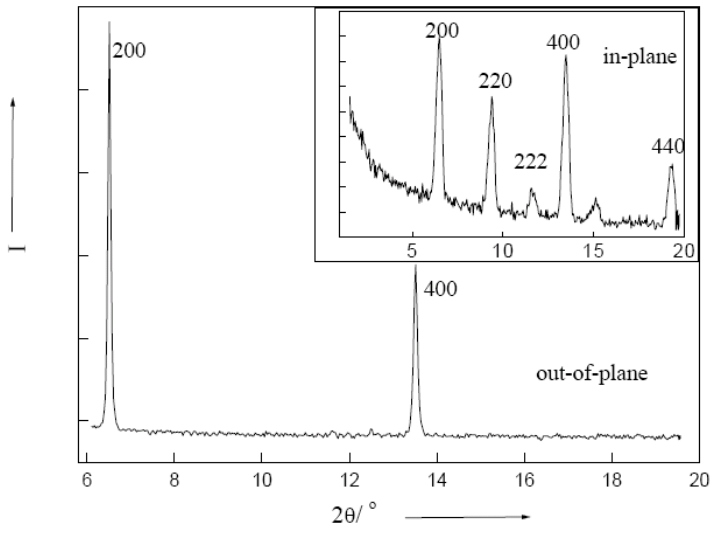

This new step-by-step route for the synthesis and growth of MOFs on organic surfaces opens up the possibility to synthesize completely new types of MOFs with compositions and structures not accessible by bulk synthesis routes, like the multi-sequential growth of two different MOFs or MOFs with two different metal ions. This new approach will also allow – at least in some cases – to provide insights in the growth mechanism of MOFs. To some extend this new approach is complementary to the growth of MOFs on organic substrates as reported recently for SAMs on Au [3, 4] and on Si [5].

Acknoledgment

We thank Dr. M. Paulus, Dr. C. Sternemann, F. Evers and Prof. M. Tolan for their assistance and support with the XRD measurements at Delta Beamline BL9.

References:

1. Shekhah O., W.H., Strunskus T. Cyganik P., Zacher D., Fischer R.A., and Wöll C. *Langmuir* 2007, *23*, 7440.
2. Shekhah et al., submitted for publication 2007.
3. Hermes, S.,Schröder, F.,Chelmowski, R.,Wöll, C., and Fischer, R.A. *J. Am. Chem. Soc.* 2005, *127*, 13744.
4. Biemmi, E., Scherb, C., and Bein, T. *JACS* 2007, *129*, 8054.
5. Zacher, D., Baunemann, A., Hermes, S., and Fischer, R.A. *J. Mater. Chem.* 2007, *17*, 2785.

Structural characterization of Co/Cr/Fe spin-valve systems

Frank Brüssing, Gregor Nowak, Katharina Theis-Bröhl, and Hartmut Zabel

Department of Physics 4, Ruhr-University Bochum, D-44780 Bochum, Germany

Spin-valves are important spintronic devices. We have chosen as a model system the trilayer Co(4 nm)/Cr(3nm)/Fe(3 nm), consisting of two ferromagnetic layers with different coercive fields separated by Cr. The sample studied was epitaxially grown [1, 2] on a MgO substrate with a 30 nm thick Cr buffer layer. It exhibits a four-fold magnetic anisotropy with the easy axis along the Fe[100] orientation. For the design of the trilayer sample we used a Cr layer thickness mediating a week antiferromagnetic coupling between the two ferromagnetic layers [3]. The final sample design is shown in Fig. 1. An x-ray source of high brilliance is indispensable for the investigation of the structural properties of such a complex system. Therefore we used the synchrotron x-ray source DELTA (BL9) at an energy of 11 keV. Figure 2 shows an x-ray reflectivity measurement of the sample. Both, the well defined oscillations and the linear drop of the intensity on a logarithmic scale indicate a high quality of the layers and interfaces as well as a very smooth surface. Rocking scans are shown in the inset which feature Yoneda wings on both sides of a narrow central peak.

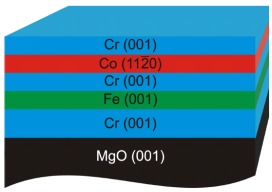

FIG. 1: Sample design

The crystalline quality of the sample in growth direction perpendicular to the sample surface is revealed by an out-of-plane high angle longitudinal scan, which is shown in Figure 3. The sharp Fe(002) and Co$(11\bar{2}0)$ peaks indicate an excellent crystal quality. The very similar lattice parameter of 2.8665 Å for Fe and 2.885 Å for Cr leads to an overlap of the Fe- and Cr-peaks resulting in one peak at $2\theta = 46.03°$. The intensity of the Fe/Cr peak is much higher than of the Co peak, which is mainly due to the thick Cr buffer layer. Furthermore, the width of the Co peak is explained by its finite thickness. These results can be taken as an indication for the good epitaxial quality of the spin valve system, but they are no prove. To ensure the quality we also investigated the in-plane structure of the trilyer system. For this we performed in-plane Bragg scans for different sample orientations as shown in figure 4-6.

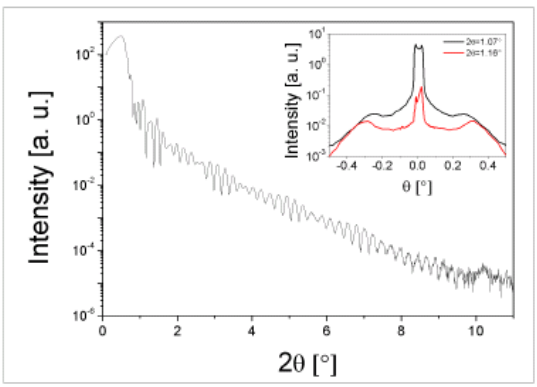

FIG. 2: Specular reflectivity

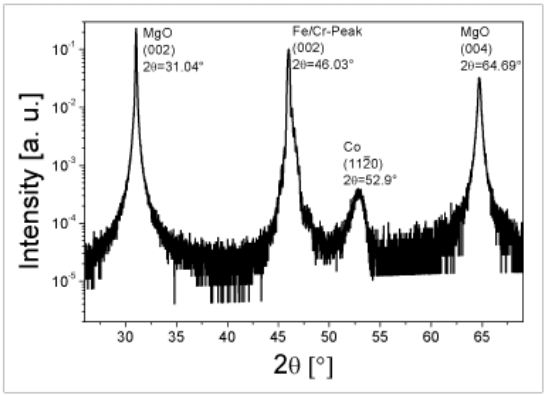

FIG. 3: High angle scan

The sharp peaks with a full width at half maximum of less than 1° is a sign for the good in-plane crystal quality of the sample.

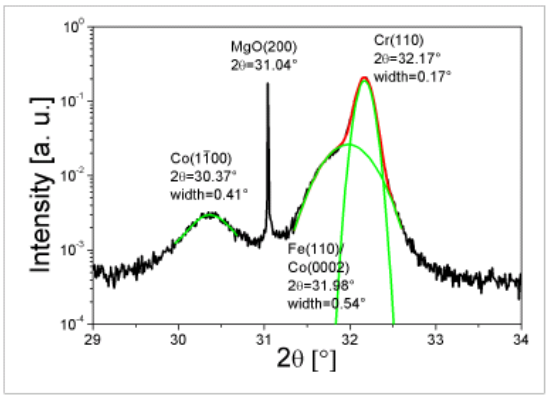

FIG. 4: In-plane Bragg scan along the MgO [100] direction

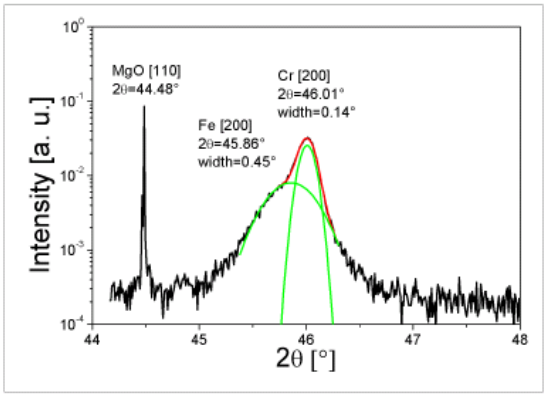

FIG. 5: In-plane bragg scan along the MgO [110] direction

Finally we investigated the epitaxial quality of the sample via in-plane rocking scans shown in figure 7. The Cr {100} and the MgO {110} in-plane axes have the same direction. So a 45° epitaxy of Cr on MgO is verified with these studies. Also a pseudomorphic growth of Fe on Cr can be recognized in these scans. The hcp-structure of the cobalt film is clearly visible in the Co in-plane rocking curves which shows 8 peaks. This is a result of two different Co $(11\bar{2}0)$ domains with an angle of 90° between each other. The reason for these two domains is the four-fold crystalline symmetry of the Cr(001) surface which offers two epitaxial orientations for the Co $(11\bar{2}0)$ layer.

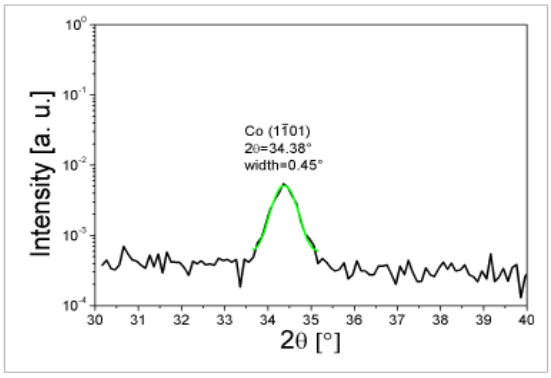

FIG. 6: In-plane Bragg scan along the Co [1$\bar{1}$01] direction

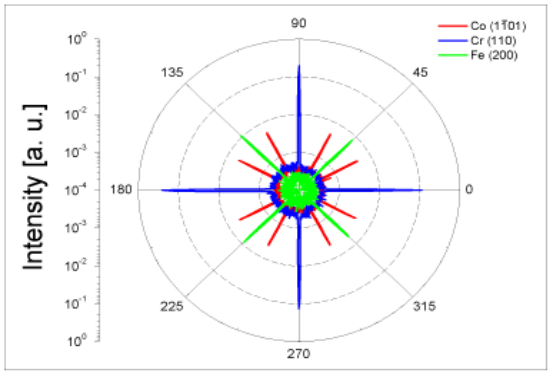

FIG. 7: In-plane rocking on Fe(200), Cr(110) and Co(1$\bar{1}$01)

These investigations show that the spin valve system Co/Cr/Fe grows in a good crystalline quality on MgO(001) with a Cr buffer layer (Fig. 1) by metal MBE methods. We are grateful to Christian Sternemann at the Beamline BL9 of DELTA for his support during this measurement. This project was supported by the SFB491.

References:

[1] K. Theis-Bröhl, I. Zoller, P. Bödeker, T. Schmitte, H. Zabel, L. Brendel, M. Belzer, and D.E. Wolf Physical Review B 57, 8 (1998)
[2] N. Metoki, W. Donner, H. Zabel Physical Review B 49, 17351 (1994)
[3] K. Theis-Bröhl, R. Scheidt, Th. Zeidler, F. Schreiber, H. Zabel, Th. Mathieu, Ch. Mathieu, B. Hillebrands Physical Review B 53, 17 (1996).

[*] Electronic address: Frank.A.Bruessing@ruhr-uni-bochum.de; URL: http://www.ep4.ruhr-uni-bochum.de

X-ray reflectivity investigations of $[Co_{60}Fe_{20}B_{20}/MgO]_n$ multilayers

Miriana Vadalá, Alexei Nefedov, Gregor Nowak, Kurt Westerholt and Hartmut Zabel

Institut für Experimentalphysik/Festkörperphysik,
Ruhr-Universität Bochum, D 44780 Bochum, Germany

Magnetic tunnel junctions (MTJs) consisting of two ferromagnetic electrode layers separated by a thin tunnelling barrier and exhibiting a large magnetoresistance at room temperature [1,2] are of great technical importance and are nowadays routinely incorporated in magnetic random access memory (MRAM) devices and magnetic sensors. For technological applications large tunneling magnetoresistance (TMR) ratios and resistance area (RA) product in the range of 1–1000 Ωm^2 are needed. Until recently most work has been devoted to junctions with AlOx barriers, where TMR values up to 70% have been observed [3]. Large TMR ratios require excellent quality of the interfaces and a small non-conformal roughness, which is known to degrade the TMR. AlOx based tunnel junctions with polycrystalline ferromagnetic metals as electrodes have conventionally been used in MTJs. Amorphous ferromagnetic electrodes, mainly consisting of alloys of 3d ferromagnets combined with Si or B, typically CoFeB, have also been already largely used. More recent results obtained with electron microscope pictures [4] suggested that the high TMR ratio is related to the electrode/barrier interface and the developing crystallization of the CoFeB on annealing at 265 °C.

Here we present a structural study of $[Co_{60}Fe_{20}B_{20}/MgO]_n$ multilayers, grown on a Si/SiO_2 substrates using the three different processes for the preparation of the MgO layers, which are commonly also applied in the literature for the preparation of the barrier. This is natural oxidation of Mg, plasma oxidation of Mg and direct sputtering of MgO. We observed the changes of the structural quality of the multilayers after annealing at different temperatures. In order to attain qualitative information about the multilayer periods, thickness fluctuations and the interface roughness, X-ray reflectivity has been used. The measurements were performed at the BL9 [5] at a fixed X-ray energy of 11 keV.

Two types of measurement were performed, namely specular and off-specular scans, with the aim to achieve information either about the multilayer structure, as well as to determine the degree of conformality of the interface roughness in a multilayer.
In Fig1. the true specular scans for different multilayers are plotted. We observe Kiessig fringes at least up to the first order Bragg peak and in some cases even beyond. Furthermore, multilayer Bragg peaks can be resolved up to the second order for the remotely oxidized multilayers and up to the third order for the naturally oxidized samples, indicating that the interfaces are relatively flat. The broadening of the third Bragg peak, visible in Fig.1d for the sample 2REMOT, must be attributed to diffuse scattering from roughness correlations. Simulations and data analysis about are still ongoing. For the natural oxidation method the annealing hardly affects the roughness parameter, whereas for the plasma oxidized samples the roughness definitely increases upon annealing. This indicates that the interdiffusion at the interfaces upon annealing is larger for the case of plasma oxidation.

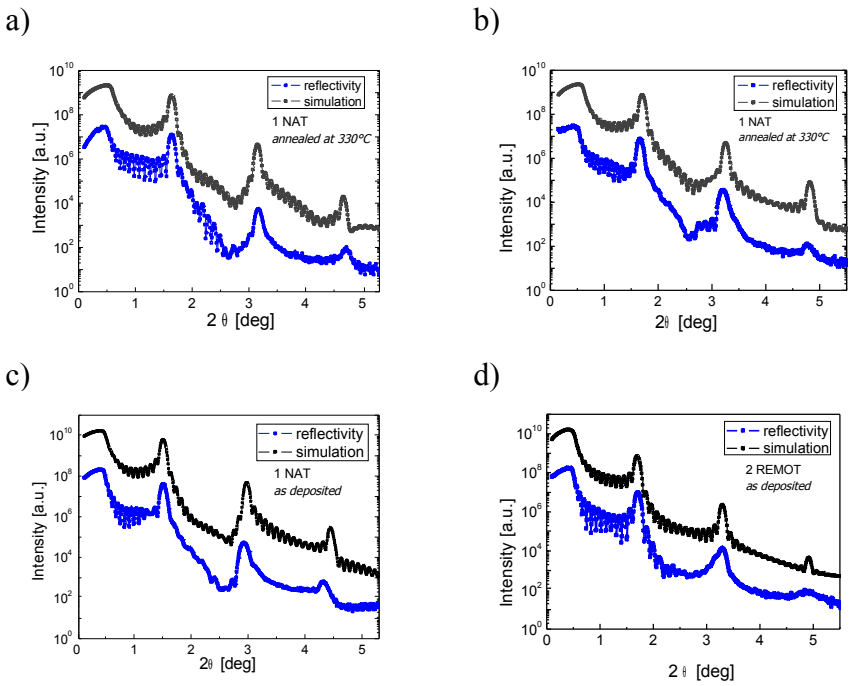

Fig. 1 Reflectivity curves and correspondent simulations for two multilayers of the series 1NAT annealed at 330° C [a) and b)] and comparison between multilayers belonging to different series both as deposited [c) and d)].

Our x-ray reflectivity results indicate that the natural oxidation of Mg at least from a structural point of view gives the highest quality layers and thus the natural oxidation should be the better technique for preparing high quality MgO barriers in magnetic tunnel junctions (MTJs).

Acknoledgment

The authors gratefully acknowledge Christian Sternemann and Micheal Paulus for their kind assistance during the experiments at the Beamline 9. The financial support provided through the European Union´s Marie Curie actions (Research Training Networks) ULTRASMOOTH under contract MRTN-CT-2003-504462 is also kindly acknowledged.

References:

[1] J. S. Moodera, L. R. Kinder, T. M. Wong, and R. Meservey, *Phys. Rev. Lett.* **74**, 3273 (1995).
[2] T. Miyazaki and N. Tezuka, *J. Magn. Magn. Mater.* **139**, L231 (1995).
[3] D. X. Wang, C. Nordman, J. M. Daughton, Z. H. Qian, and J. Fink, *IEEE Trans. Magn.* **40**, 2269 (2004).
[4] F. F. Li, R. Sharif, L. X. Jiang, X. Q. Zhang, X. F. Han, Y. Wang, and Z. Zhang, *J. Appl. Phys.* **98**, 113710 (2005).
[5] C. Krywka, M. Paulus, C. Sternemann, M. Volmer, A. Remhof, G. Nowak, A. Nefedov, B. Pöter, M. Spiegel, and M. Tolan, *J. Synchrotron. Rad.*, **13**, 8 (2006).
[6] M. Vadalà, M. Wolff, K. Westerholt, H.Zabel, P. Wisniowski, S. Cardoso, *submitted to Acta Physica Polonica*

Protein-Protein Interactions Modulation : A Potential Candidate for Inhibiting Amylodogensis

Nadeem Javid[a], Karsten Vogtt[a], Christina Krywka[b], Metin Tolan[b] and Roland Winter[a]

[a]University of Dortmund, Department of Chemistry, Physical Chemistry I – BiophysicalChemistry, Otto-Hahn Str. 6, D-44227 Dortmund, Germany
[b]University of Dortmund, Fachbereich Physik / DELTA, D-44221 Dortmund, Germany.

The intermolecular interaction potential of amyloidogenic-prone insulin was evaluated at different protein concentrations by using synchrotron small-angle X-ray scattering in combination with liquid state theoretical approaches. The experimentally derived static structure factors obtained without and with added NaCl were analyzed with a statistical mechanical model based on the DLVO potential which accounts for repulsive and attractive interactions of the protein molecules. The data reveal that insulin particles selfassemble into equilibrium clusters with a concentration-dependent aggregation number and cluster size distribution instead of forming a homogeneous spatial distribution, even at low concentrations. The depth of the attractive intermolecular interaction potential $V_W(r)$ is a factor of about 10 deeper than for lysozyme (Figure 1), representing a stable native protein, and exhibits a different concentration dependence, indicating that short-range van der Waals and specific hydrophobic attractions are strong already at rather low protein concentrations. Upon charge screening of the positively charged insulin with 0.1 M NaCl, a drastic increase of the attractive well depth J is observed, hence explaining the enhanced rate of protein aggregation and fibrillation under charge-screening conditions. To reveal how the intermolecular interaction depends on solvational conditions and the initial aggregation-prone species, we carried out additional experiments at conditions, where insulin exists as monomeric species, only. The data reveal that the well depth is slightly (10%) smaller, reflecting a significant delay of the nucleation process of insulin fibrillation, however. An enhanced hydrophobicity of the solvent (by adding EtOH) partially balances the hydrophobic part of attractive interaction between the protein molecules, thus slightly disfavoring short-range attractive protein-protein interactions. Surprisingly clearly, the method employed here is able to distinguish the striking differences regarding interaction forces between aggregation-prone proteins such as insulin in the pre-aggregated regime and natively stable globular proteins, which might be used in forthcoming studies on other, disease-related amyloidogenic proteins.

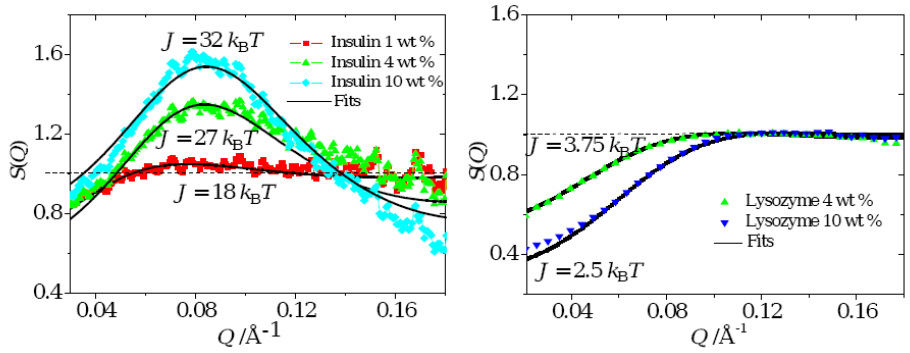

Figure 1: Experimental and calculated (full lines in black) structure factors S(Q) for different concentrations of insulin (1 wt% (squares), 4 wt% (upward triangles), 10 wt% (diamonds)) in water at pH 2. b) Experimental and calculated (full lines in black) S(Q) for different concentrations of lysozyme (4 wt% (upward triangles), 10 wt% (downward triangles) in 20 mM citrate buffer at pH 4.6). For clarity only one experimental point in six is displayed.

N. Javid, K. Vogtt, C. Krywka, M. Tolan, R. Winter, Phys. Rev. Lett. **99**, 028101 (2007)

Solution-SAXS – proteins at extreme conditions

C. Krywka[1], R. Winter[2], M. Tolan[1]

[1]DELTA, Department of Physics, University of Dortmund, Germany
[2]Department of Physical Chemistry,University of Dortmund, Germany

christina.krywka@uni-dortmund.de

The biological activity and the chemical properties of proteins are strongly influenced by both the structure of the aqueous microenvironment and the thermodynamic parameters. Understanding the effects of various types of cosolvents on the structure and dynamics of proteins is crucial for a deeper insight into protein stability, folding, aggregation and fibrillation processes. The latter play an important role in many conformational diseases, such as Alzheimer, Huntington, Creutzfeldt-Jakob, and Parkinson. Recently, we could show that these fibrillation processes are in fact strongly influenced by the type and concentration of cosolvents [1-5]

In order to determine the effect of different types of cosolvents (stabilizing or destabilizing) on the native and unfolded states of the model protein Staphylococcal Nuclease (SNase) we have performed SAXS measurements at temperature and pressure conditions where unfolding of the protein sets in. The experimental equipment which had to be developed in the course of the ongoing project comprises of a high-pressure, temperature controlled sample environment (see Fig. 2) bearing the ability to perform SAXS-measurements on liquid samples at pressures up to 7 kbar in a wide temperature range (-15°C to 80°C). From the evaluation of the measured radii of gyration (R_G) we could determine the effects of the cosolvents glycerol, sorbitol, urea, trimethylamine-N-oxide, tetrafluorethylene, and K_2SO_4 on the native and pressurized states of the protein. Examples of the measured data are shown in Fig. 1.

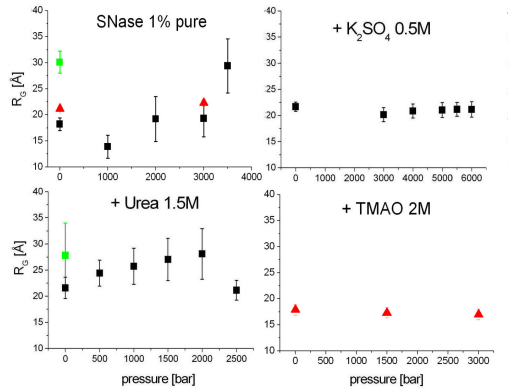

Fig. 1: Pressure dependent radii of gyration (R_G) in presence of different type of cosolvents at T=25°C. ■=APS data, ▲=DELTA data. Green markers indicate data at T=65°C.

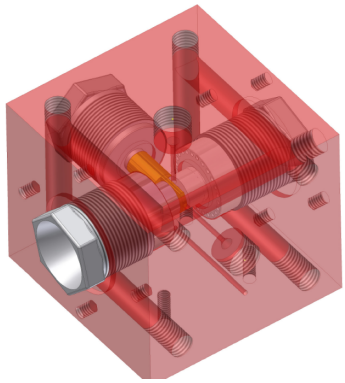

Fig. 2: 3D-model of the recently developed high pressure sample environment used at BL9 of DELTA

References:

[1] S. Grudzielanek, R. Jansen, R. Winter, J. Mol. Biol. 351 (2005) 879; ibid 356 (2006) 497
[2] N. Javid, K. Vogt, C. Krywka, M. Tolan, R. Winter, Chem. Phys. Chem. 8 (2007) 679
[3] N. Javid, K. Vogt, C. Krywka, M. Tolan, R. Winter, Phys. Rev. Lett. 99 (2007) 028101
[4] W. Dzwolak, R. Ravindra, R. Winter, PCCP 6 (2004) 1938
[5] W. Dzwolak, R. Ravindra, J. Lendermann, R. Winter, Biochemistry 42
[6] C. Krywka, C. Sternemann, M. Paulus, N. Javid, R. Winter, A. Al-Sawalmih, S. Yi, D. Raabe, M. Tolan, J. Synchrotron Rad. (2007). 14, 244

Investigation of the lattice strain evolution in tension and compression of different phases in the mineralized lobster cuticle

C. Sachs[1], S. Yi[2]

c.sachs@mpie.de, sangbong.yi@tu-clausthal.de

[1.] Max-Planck-Institut für Eisenforschung, Max-Planck-Str. 1, 40237 Düsseldorf, Germany
[2.] Clausthal University of Technology, Institute of Materials Science and Engineering, Agricolarstr.6, 38678 Clausthal-Zellerfed, Germany

Introduction

The cuticle of the lobster consists of three structurally different layers: an outermost epicuticle and an inner procuticle which comprises the exocuticle and the endocuticle. The epicuticle is a thin waxy layer which provides a permeability barrier to the environment. The mechanically relevant layer is the procuticle which is made up of mineralized chitin-protein fibers forming lamellae. Among other factors the structure and the resulting mechanical properties of the exocuticle and the endocuticle are defined by the grade of mineralization and the stacking height of the twisted plywood structure also referred to as Bouligand structure. In the hierarchical organization the basic structural units are crystalline nanofibrils which are made up of eighteen to 25 anti-parallel α-chitin chains wrapped with proteins and subsequently cluster to form chitin protein fibers. The α-chitin phase has an orthorhombic crystal structure with the lattice parameters a = 4.74 ± 0.02 Å, b = 18.86 ± 0.01 Å, c = 10.32 ± 0.04 Å, and $\alpha = \beta = \gamma = 90°$. By arranging the fibers parallel in horizontal planes and rotating gradually superimposed layers of these planes around the normal axis of the cuticle, a twisted plywood structure or Bouligand structure is created. Additionally, the fibers are arranged around cavities originating from an extremely well developed pore canal system of the lobster which gives the structure a honeycomb-like appearance. The objective of our study is to gain a better understanding of the underlying microscopic deformation mechanisms of the different phases present in the endocuticle of the lobster *Homarus americanus*. Due to its complex nano-composite structure, standard investigation methods cannot be applied to the individual components. Hence, wide-angle X-ray diffraction using synchrotron radiation is an excellent alternative to examine the microscopic deformation mechanisms which is also non-invasive and non-destructive.

Experiments

The specimens used for the tests were taken from the chelipeds of a large adult, non-molting American lobster (*Homarus americanus*). Two sets of samples were dissected from the pincher and the crusher claw. One set was air-dried while the other one was stored at low temperatures in a humid atmosphere (4°C, >90% R.H.) in order to prevent desiccation. The samples designated for tensile testing were machined to bone-shaped test specimens (2 mm thickness, parallel length of 4 mm x 2mm, 22 mm total length). The samples designated for compression testing were machined to tetragonal test specimens (2mm x 2mm x 3mm). Before testing the white sample surfaces were decorated with a graphite aerosol spray to create a stochastic black spot pattern for better contrast as required for digital image correlation. During testing the wet samples were kept moist by placing a wet sponge underneath them.

The in-situ compression and tensile tests were performed on a special miniaturized test rack constructed by Kammrath & Weiss GmbH (44141 Dortmund, Germany). The computerized device features two moveable crossheads allowing the sample to remain in a stable centered position during testing. The maximum capacity of the used load cell amounts to 1000 N. The testing machine was mounted horizontally to a x-y-z coordinate table in the Eulerian cradle at the synchrotron beam line BL9 at DELTA (Fig. 1). The specimens were strained stepwise in intervals of 15 µm in tension and compression with 1.0 µm/s until failure. After each deformation step a set of Debye-Scherrer rings was repeatedly registered using the MAR345 image plate. Since the full Debye-Scherrer rings were recorded on the image plate, the lattice strain evolution along as well as that perpendicular to the loading direction could be measured simultaneously. The beam energy amounted to 15.5 keV, corresponding to the wavelength of 0.8Å, and the beam size was set to 1.2 x 1.2 mm². In order to record the deformation, images were taken using a digital camera which was mounted on a support positioning it perpendicular to the tensile test rack. The camera set-up is controlled by the ARAMIS system (GOM - Gesellschaft für Optische Messtechnik mbH, 38106 Braunschweig, Germany). Digital pictures were taken at the initial state and after each deformation step to determine the macroscopic strain.

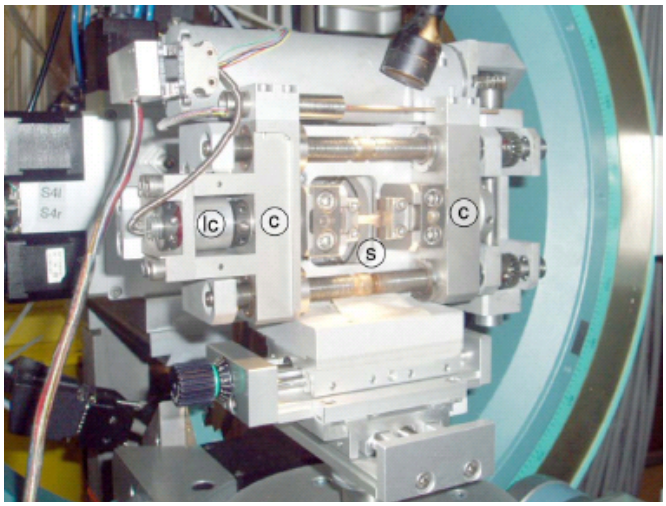

Fig. 1. Miniaturized tensile test rack with two moveable crossheads (c) and 1000 N load cell (lc) inside the Eulerian cradle. The test specimen (s) is mounted in the center.

Fig. 2 shows a detector image and the diffraction profile obtained by the summation along the radial direction of the Debye-Scherrer (D.-S.) rings. The inhomogeneous intensity distribution along the D.-S. rings indicates the strong crystallographic texture in the material which causes the difficulty during the data evaluation. For example, the {040} reflection has strong intensity in the loading direction (L.D.), while very weak intensity of the reflection is observed in the perpendicular direction to L.D. (P.D.). However, it must be noted that the characteristics of the lattice strain for almost all reflections can be achieved by combining the data sets from different sampling directions. The lattice strain is calculated by the following equation:

$$\varepsilon = \frac{d^{hkl} - d_0^{hkl}}{d_0^{hkl}} ,$$

where d_0^{hkl} represents the unstrained inter-planar spacing. As a preliminary result, the relationship between the macroscopic stress which was applied to the sample and the resulting lattice strain of α-chitin is given in Fig. 3. Three pairs of specimens were tested under different loading conditions in the dry state. During compression in transverse and normal direction a similar behavior of the lattice strains is observed, i.e. the evolution of the lattice

strain is independent on the initial status of the crystallographic texture. The lattice strain along the crystal b-axis, 040 reflection, reaches a relatively small value of about 0.2% up to 150 MPa which corresponds nearly to the stress to fracture. In contrast, a larger lattice strain along the crystal c-axis, 002 reflection, can be seen during the compression as well as the tensile loading. A lattice strain of ± 0.6% is already reached at a macroscopic stress below 40 MPa. The above experimental observations indicate the strong anisotropic response of each crystallographic direction to the macroscopic stress, so called strong mechanical anisotropy depending on the crystal direction. The anisotropy ratio between the 'hard' direction (040 reflection) and the 'soft' direction (002 reflection) amounts to a factor of three. It is strongly expected that better insight into the mechanical response of the material can be achieved by profound understanding of these interesting phenomena.

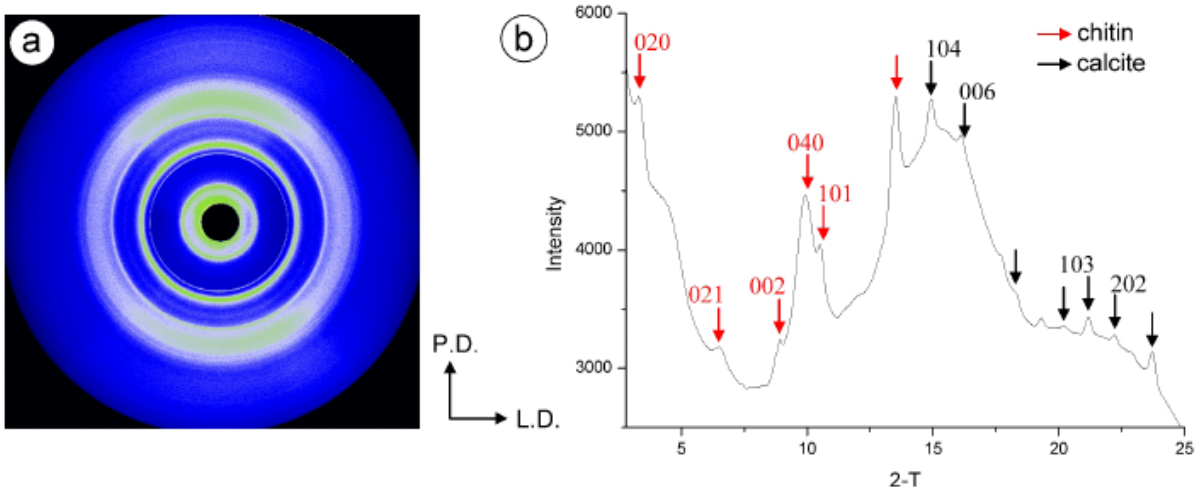

Fig. 2. Detector image (a) and summed diffraction profile along the radial direction of the detector image (b).

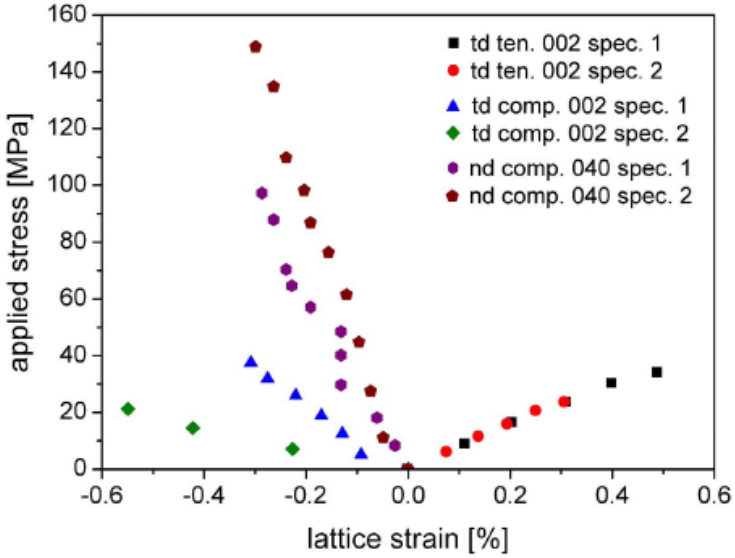

Fig. 3. Relationship between the lattice and the applied stress for pairs (spec. 1, 2) of specimens tested in transverse (td) and normal (nd) direction in the dry state. In transverse direction the samples were loaded both in tension (ten) and compression (com) while loading mode in the normal direction is solely compression (com). The data were obtained from the 002 reflection in the transverse direction and from the 040 reflection in the normal direction.

XSW measurements of ion distributions above a charged surface

M. Brücher[1], A. von Bohlen[1], C. Sternemann[2], M. Paulus[2], R. Hergenröder[1]

[1] ISAS Dortmund, Bunsen-Kirchhoff-Str. 11, 44139 Dortmund
[2] DELTA, Technische Universität Dortmund, Maria-Goeppert-Mayer-Str. 2, 44221 Dortmund

An important parameter for the characterisation of surfaces is the electrostatic potential by surface charges. Closely related to this is the amount and character of species near the liquid/ solid interface which are crucial for the description of transport or electrochemical phenomena. For the experiments presented in this report, X-ray standing waves (XSW) were used to analyse the potential at a solid/liquid interface by measuring the distribution of marker ions above a silicon wafer.
The work is performed in the framework of an EU-funded project (Influss, FP-6) dedicated to the study of modification of polymers, glass, and similar materials potentially useful for microfluidic applications.

Principle of XSW measurements

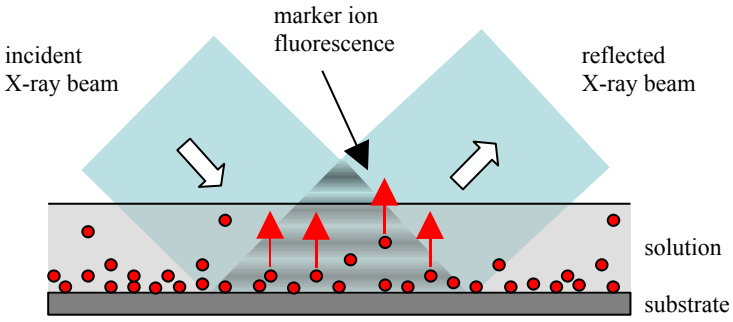

Fig.1: Schematic illustration of XSW field generated by interference of incident and reflected beam.
At the positions of maxima (constructive interference), ions are excited to emit fluorescence.

As depicted in fig. 1, the interference of incident and reflected beam causes an XSW-field above the reflecting surface. The positions of nodes and antinodes depend on the angle of incidence. At a specific angle α, only the ions at the positions of XSW maxima emit fluorescence, so by varying α the ion distribution of the solution can be scanned horizontally.

Sample Preparation

As reflecting substrates, silicon wafers were used. The surface charge was modified by a coating of aminosilane, whose $-NH_2$ groups reacted to $-NH_3^+$ in aqueous solution, causing a positive surface charge.

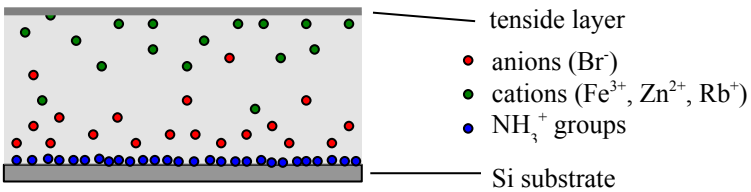

Fig. 2: Illustration of ion distribution in a thin (some µm) liquid film. Cations are repelled; anions are attracted by the positive surface charge. A tenside layer prevents the film of evaporation.

Three solutions were prepared, each containing Br, Rb, or Fe as marker atom and Zn as an impurity (probably from wafer impurities). Additionally, the solutions were prepared under acid and basic conditions by adding nitric acid (pH value of the solution: 2.8) and sodium

hydroxide (pH value: 10) respectively. The different pH values were intended to modify the surface charge. The Concentration of Br, Rb and Fe ions was 1g/l, a thin tenside film prevented the solution film (thickness some µm) of evaporation or degradation.

Experiments and Results

The experiments were performed at the SAW beamline BL9, using the energy of 15.5 keV. A simulation program was developed to calculate XSW intensity according to a given ion distribution model (e.g. Helmholtz, Gouy-Chapman).

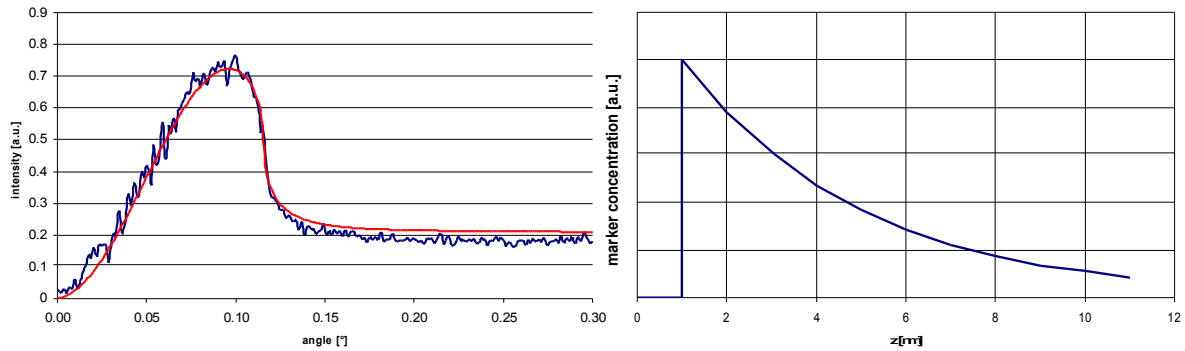

Fig. 3: Left: XSW scan of Br^- in water film above a positively charged surface. Red line: simulation. Right: Model of anion distribution used for simulation, exponential decay of ion concentration.

In neutral and acid solutions, anions generally were attracted and cations were repelled by the potential of the positive surface charges. In basic solutions, Fe and Zn precipitated as hydroxides, forming a thin layer above the substrate.

In a next step, we intend to perform XSW measurements using other types of substrates, as glass or polymers like PDMS or PMMA. Furthermore, we project to analyse the effect of surface modifications on the potential at the solid/liquid interface.

Lysozyme Adsorption at the Silica/Water Interface: an in-situ High Energy X-ray Reflectivity Study

Florian Evers, Kaveh Shokuie, Michael Paulus, Christian Sternemann, and Metin Tolan

Experimentelle Physik I / DELTA, Technische Universität Dortmund, Maria-Goeppert-Mayer-Str. 2, 44221 Dortmund

Lysozyme adsorption at the silica/water interface has been studied using high energy x-ray reflectivity which is a well-established means to study the structure of thin films. Data on thin protein layers at solid/liquid interfaces are still rare. The dispersion profile of adsorbed lysozyme layers at hydrophilic silica interfaces, the effect of pH and protein concentration of the aqueous solution on the adsorption, and the time-dependence of the adsorption process were studied. The adsorption of lysozyme monolayers is observed which is partially in contrast to former measurements.

Introduction

Studying protein adsorption onto solid surfaces is not only of considerable academic interest, but also of great practical importance [1]. Interactions of proteins with solid surfaces are major issues in a number of fields of research such as medicine, biotechnology or food processing. For instance, lysozyme is one of the main components of the tear liquid. Contact lenses are affected by the formation of a lysozyme biofilm that can lead to immunological reactions and inflammation of the eye [1]. Whenever an aqueous protein solution is exposed to a solid surface, protein molecules will generally tend to adsorb spontaneously at the solid/liquid interface. The driving forces for protein adsorption are of both entropic and enthalpic character. The degree of protein adsorption at solid surfaces is influenced by the nature of the protein solution that is, e.g., the structure of the protein, the solution pH, the ionic strength of the solution, the protein concentration or the temperature. Moreover it is affected by the nature of the solid substrate, including its hydrophobicity and polarity [1]. Lysozyme is a globular protein with an ellipsoidal shape ($30 \times 30 \times 45$ Å^3), has a molecular weight of 14 kDa and an isoelectric point (pI) of 11. As lysozyme is a robust model protein with a well-known structure, its adsorption onto solid surfaces is an area of current research [2, 3]. Using high energy x-ray reflectivity (HEXRR), the effects of solution pH and concentration on lysozyme adsorption at the silica/water interface were examined. HEXRR is a unique technique for the investigation of buried solid/liquid interfaces [4].

Experimental section

The high energy x-ray reflectivity measurements were performed using the reflectivity setup of beamline BL9 at DELTA (E =27 keV), as described in [4]. The sample cell with a volume of about 5 cm^3 has two Kapton windows for beam entrance and exit, as depicted in Fig. 1. The wafer is placed at the bottom of the cell and fixed with a bar. The reflectivity of pure water on the Si surface is measured for each wafer and serves as a reference for further measurements. Then the aqueous protein solution is filled into the cell and the reflectivity of the system is measured.

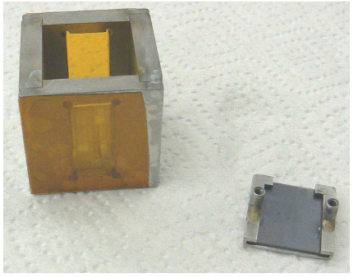

FIG. 1: The small sample cell for the investigation of solid/liquid interfaces. The bar which holds the wafer is placed besides the sample cell [4].

Lysozyme (from chicken egg-white) was purchased from Sigma (Taufkirchen, Germany). Protein solutions were prepared using 10 mM phosphate buffer. The solution pH was adjusted by adding NaOH or HCl. Silicon wafers were purchased from Wacker Siltronic (Burghausen, Germany). They were cut into pieces of 18 × 18.8 mm^2 and cleaned with piranha solution. All experiments were performed at room temperature.

Results and discussion

Effect of pH:

Protein solutions with different pH were prepared at constant lysozyme concentration of 0.1 mg/mL. All reflectivity curves can be refined assumming a one-layermodel. The native oxide layer of the silicon wafers does not have a remarkable impact on the fit. First results of the dispersion and the roughness of the silicon substrate and the dispersion, the thickness and the roughness of the lysozyme layer are shown in Tab. I; experimental data and refinement for pH 7 are exemplarily displayed in Fig. 2, the corresponding dispersion profile is depicted in Fig. 3. It is theoretically predicted that maximal adsorption

pH	$\delta_{Si}[10^6]$	σ_{Si}[Å]	$\delta_{Lys}[10^6]$	d_{Lys}[Å]	σ_{Lys}[Å]
4	0.69	1.9	0.38	23.7	8.6
7	0.69	2.2	0.41	26.5	7.0
11	0.70	2.1	0.38	29.3	7.0

TABLE I: Structural parameters obtained assuming monolayer adsorption; measured at E = 27 keV.

occurs at the isoelectric point (pI = 11). This tendency is corroborated by our measurements. Neutron reflectivity data suggest adsorbed layers of 35 Å to 60 Å for similar solution conditions and are interpreted as sideways-on, end-on or bilayer adsorption [2]. In contrast an interpretation of lysozyme adsorption as monolayer formation is required in order to explain the thickness of the adsorbed
layer observed in this work.

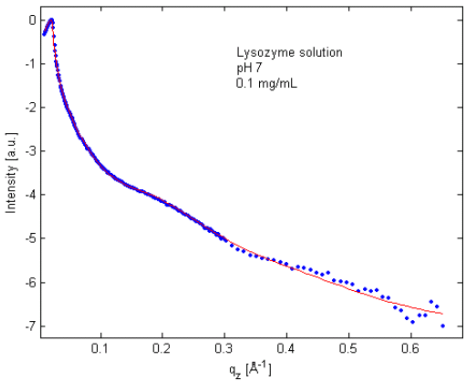

FIG. 2: X-ray reflectivity curve of the aqueous lysozyme solution/silica interface with lysozyme solution of pH 7 and 0.1 mg/mL (blue points). The solid curve (red) shows the refinement of the data, the corresponding dispersion profile is displayed in Fig. 3.

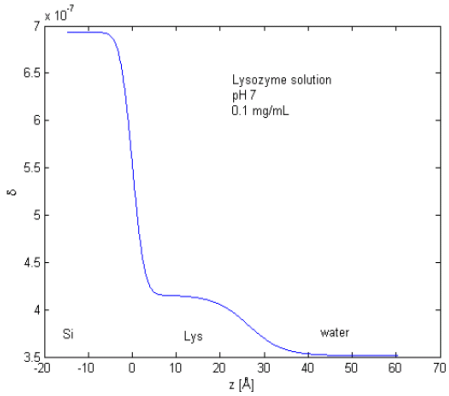

FIG. 3: Dispersion profile of the aqueous lysozyme solution/silica interface, obtained by a refinement of the reflectivity data shown in Fig. 2.

Adsorption kinetics:

At low lysozyme concentration of 0.03 mg/mL adsorption kinetics were studied by fast reflectivity scans. Results are shown in Fig. 4. The red curve shows the reflectivity curve of water on the wafer. The first scan was taken seven minutes after the insertion of the protein solution.

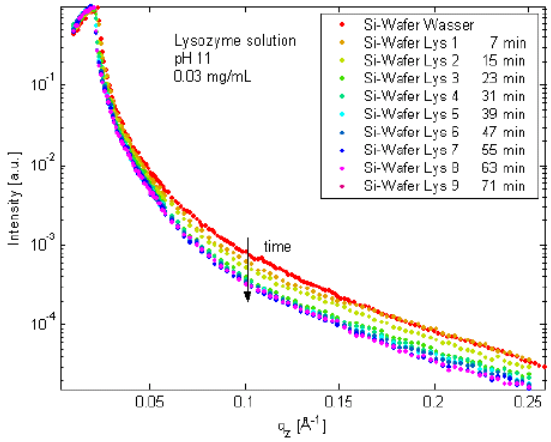

FIG. 4: Time-dependent effects: Fast x-ray reflectivity curves of the aqueous lysozyme solution/silica interface with lysozyme solution of pH 11 and 0.03 mg/mL. Data points shown in different colours according to the inset. Equilibrium is reached after about 60 minutes.

Each scan took about eight minutes. Obviously an equilibrium is reached after about 60 minutes. We would like to thank the DELTA machine group for providing synchrotron radiation and technical support.

References:

[1] C. Czeslik, Z. Phys. Chem. 218, 771 (2004).
[2] T.J. Su et al., J. Coll. Interf. Sci. 203, 419 (1998).
[3] G. Jackler et al., Langmuir 18, 6565 (2002).
[4] M. Paulus et al., subm. to J. Syn. Rad. (2007).

Hydrate formation in the system CO2-water: High energy x-ray scattering

Felix Lehmkühler, Michael Paulus, Christian Sternemann, Daniela Lietz, and Metin Tolan

Fakultät Physik/DELTA, Technische Universität Dortmund,
Maria-Goeppert-Mayer-Str. 2, D-44221 Dortmund

We report an investigation of the hydrate formation in the system water-CO2. X-ray reflectivity measurements at the water-CO2 gas interface show only a pressure dependent adsorption of gas molecules on the water surface. Rising the gas pressure until a macroscopic layer of liquid CO2 condenses at the water surface hydrate formation can be observed. X-ray diffraction at different postions of the sample yields the highest hydrate formation rate at the interface water-liquid CO2.

1. Introduction

Clathrates are structures where a guest molecule is enclosed into a cage network. In the case of hydrogen bond water cages with embedded gas molecules these structures are called gas hydrates. They are common in nature, e.g. methane hydrates in ocean floor or permafrost regions and are usually formed at low temperatures and high pressures. Furthermore, hydrates are promising candidates for future energy recovery and hydrogen storage [1]. CO_2 hydrate in particular can potentially be used for CO_2 recovery from flue gas or for deep ocean storage of CO_2 emitted from power plants [2, 3]. CO_2 forms the cubic structure I (sI) hydrate with a lattice constant of 11.98 Å and a stoichiometry of $(H2O)_{46}(CO2)_8$. The induction time $t_i \approx 2h$ of CO_2 hydrate formation is low compared to other gases. At 0°C the minimum pressure for stable CO_2 hydrates is 12.5 bar.
Although hydrates have been in the focus of different experiments during the last 50 years the microscopic formation process of hydrates is still not understood. Three different theories for this process are proposed in the literature: the cluster nucleation theory [1], the local structuring hypothesis [4], and a surface driven model [5]. The first and the second model explain the formation as a bulk process. In the framework of the cluster nucleation theory small water-guest cluster form immediately after dissolution of gas molecules, agglomerate and finally the nucleation sets in. The local structuring hypothesis predicts the formation of hydrates after stochastic arrangements of the dissolved guest molecules in the water similar to the hydrate structure is achieved. In contrast the surface driven model bases on the high gas concentration at the water surface. Due to the high offer of gas molecules hydrate cluster form, grow and agglomerate.

2. Experimental methods

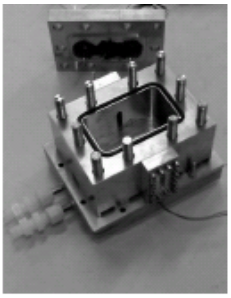

Figure 1: Sample cell.

The low induction time, high dissolubility of CO_2 in water, and thus the possibility for hydrate formation at the water surface or in the bulk, the system CO_2-water is an ideal sample to study the hydrate formation in-situ. To investigate such a formation at the water surface x-ray reflectivity measurements were performed. The formation of CO_2 hydrate in the bulk was observed by x-ray diffraction. Due to the high pressures where hydrate formation takes place a sample cell with stainless steel walls of 2 cm thickness was constructed, see Fig. 1. With this cell, experiments up to the condensation pressure of CO_2 of 35 bar at 0°C are possible to perform. Two 1 mm aluminium windows allow the x-ray beam to penetrate the cell. This makes the use of high energy x-rays necessaryt. High energy x-ray reflectivity

measurements (E = 72.5 keV) of the water-CO_2 interface performed at ID15 at ESRF [6] show adsorption of thin CO_2 films at the water surface in agreement with adsorption theory [7]. However, no hydrate formation after 6-8 hours waiting at pressures 2.5 times above the minimum pressure for CO_2 hydrate could be observed. After rising the pressure above 35 bar for condensing a macroscopic liquid CO_2 layer of several mm thickness, small hydrate clusters could be detected at the water-liquid CO_2 interface. Bragg reflections measured at the interface occur and disappear continuously, see Fig. 2. High energy diffraction (E = 27 keV) at BL9 at DELTA [8] were performed to examine this formation more precisely. In contrast to the measurements at the ESRF where a point detector was applied, a MAR345 image plate could be used as detector. This allows to measure the whole spectrum at once and investigate the occurrence and disappearence of different Bragg reflections simultaneously. The measurements where performed at different sample positions to determine whether the hydrate formation takes only place at the water-liquid CO_2 interface or additionally at other positions, e.g. the water bulk or the bottom of the sample cell.

3. Data analysis and discussion

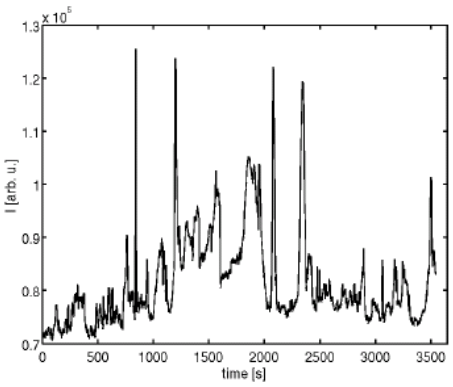

Figure 2: Timescan of the (321) Bragg reflection.

A

Figure 3: MAR345 image of the water-CO_2 interface.

MAR345 image taken from the water-liquid CO_2 interface is shown in Fig. 3. Bragg peaks according to a CO_2 hydrate diffraction pattern are clearly visible as black dots. Due to the narrow slits where the steel cell can be penetrated, the dots are visible only at a small area. The strong diffraction rings stem from the aluminium windows. Besides, the water-CO_2 interface, images were taken at the water bulk, liquid CO_2 bulk, liquid CO_2 surface, and the gas phase. The integrated spectra are presented in Fig. 4. The spectra are normalized to the large aluminium windows. Besides, the water-CO_2 interface, images were taken at the water bulk, liquid CO_2 bulk, liquid CO_2 surface, and the gas phase. The integrated spectra are presented in Fig. 4. The spectra are normalized to the large aluminium peak at $2\theta \approx 10°$. It is clearly visible that the highest amount of hydrate can be detected at the water- CO2 interface followed by the bulk water and bulk CO_2. At the surface of the liquid CO_2 only few peaks and in the gas phase no peaks are measured respectively. Unfortunately, the area where hydrate peaks can be expected is quite large because of the sample thickness of 8 cm. Thus, a broad peak instead of a few small peaks is visible. Furthermore, it can be deduced that small single crystals of CO_2 hydrate form due to the isolated peaks instead of rings visible on the MAR images. Further data analysis is still in process. In summary, we observed the formation of CO_2 hydrate with preference at the liquid CO_2-water interface. More measurements with an improved sample cell (sample thickness of a few mm) will follow during the next months.

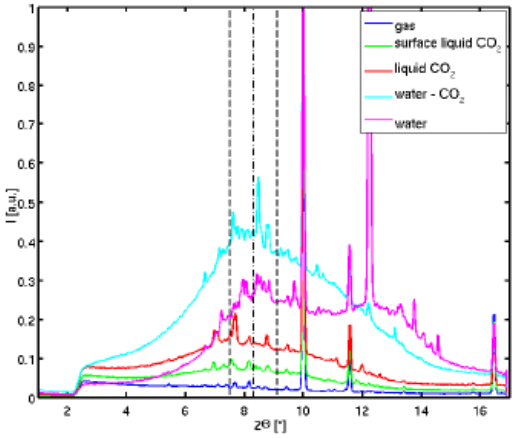

Figure 4: Integrated spectra of different height positions. Dashed lines show the area where the largest CO_2 hydrate peak is expected. The large peaks and some small ones observable in every spectrum have their origin in the aluminum windows and can be used for calibration.

Acknoledgment

We thank the DELTA machine group for providing synchrotron radiation and the ID15 crew at ESRF for supporting our beam time.

References:

[1] E.D. Sloan Jr., Nature 426, 353 (2006).
[2] S.P. Kang and H. Lee, Environ. Sci. Technol. 34, 4397 (2000).
[3] R.P. Warzinski et al., Annals of the New York Academy of Science 912, 226 (2000).
[4] R. Radhakrishnan and B.L. Trout, J. Chem. Phys. 117, 1786 (2002).
[5] B. Kvamme, Annals of the New York Academy of Scienc , 912, 496 (2000).
[6] V. Honkimäki et al., J. Synch. Rad. 13, 426 (2006).
[7] M. Paulus, C. Gutt, and M. Tolan, Phys. Rev. E 72, 061601 (2006).
[8] C. Krywka et al., J. Synch. Rad. 13, 8 (2006).

STATUS OF THE VUV-BEAMLINES U55 (BL11) AND TGM (BL12) AT DELTA

Ulf Berges, Sven Döring, Christian Flüchter, Martin Schmidt, Frank Schönbohm, Daniel Weier, and Carsten Westphal

berges@delta.uni-dortmund.de

DELTA, Technische Universität Dortmund, Maria-Goeppert-Mayer Str. 2, Dortmund, Germany
Fachbereich Physik, Technische Universität Dortmund, Otto-Hahn-Str. 4, Dortmund, Germany

The VUV/soft x-ray beamlines TGM (BL12) and U55 (BL11) at the storage ring DELTA are set up by the physics department of the Technische Universität Dortmund. Commissioning of both beamlines and support is provided by the physics department, while beamline access is available for internal and external researchers of the university. As a summary of last year's activities, the commissioning of beamline 11 was nearly completed when a venting accident happened in September 2006. Thus, major work-force was concentrated on a recovery of BL 11 and the commissioning of BL12 was interrupted. Now, BL11 is operational again, still with some necessary commissioning due to new settings as a consequence of the repair tasks on the refurbished components.

U55-Beamline

The energy range of the U55-Beamline is from hυ = 55 to 1500 eV, accepting linearly polarized synchrotron radiation emitted by the permanent magnet undulator U55 with a variable gap from 20 to 300 mm. A plane grating monochromator (PGM) is integrated in the beamline with two gratings of 400 and 1200 lines/mm for high flux and high resolution experiments, respectively. In the case of high flux experiments, about 10^{12} photons/s are reached for an exit slit of 200 µm at 100 mA stored electron beam. The calculated maximum energy resolution is 30000, if the exit slit size is reduced to 20 µm width, with a reduced photon flux of 10^{10} to 10^{11} photons/s/0.1A. The calculated focus size is 70 x 30 μm^2 at the experiment.

BL 11 is operational again since May 2007. Since then photoemission spectroscopy (XPS), angle scanned photoelectron diffraction (XPD), and x-ray standing wave experiments (XSW) were performed, parallel to the necessary commissioning of the new set-up. The XSW-experiments were performed on various samples as B_4C and W, GaAs and AlAs multi-layers, Si and $MoSi_2$ multilayers, $SrTiO_3$ and $La_{0,7}Sr_{0,3}MnO_3$ or MgO and Fe wedge above a GaAs and AlAs multilayer. The scientific results of these experiments are presented in the report of S. Döring. F. Schönbohm presents XPS- and XPD-measurements of zirconium oxide on Si(100) performed at this beamline in his report.

TGM-Beamline

The TGM-Beamline is accepting synchrotron radiation from a dipole magnet within the energy range from hυ = 6 to 200 eV. The beamline is intended for investigations on magnetic systems containing Fe, Co, and Ni-compounds since the 3d electron binding energies of those elements are in that energy range. In a further step we plan to record Fermi-surfaces.

Presently, the beamline is under commissioning. First measurements of the photon flux at the experiment were performed with a photodiode and gas cell. Figure 1 displays the photoionization spectrum of the Xe $4d_{5/2}$ $4d_{3/2}$ to 6p 7p transition, recorded with the 600 lines/mm grating. Figure 2 shows a photoionization spectrum of He, taken with the same grating. The second grating with 1800 lines/mm is under commissioning. Further spectra of Kr and Ar are necessary to perform an energy calibration within the complete energy range of this beamline. These first two spectra were recorded in October 2007, the final set-up of the beamline and the optimization for maximum flux and resolution will be carried out within the next months.

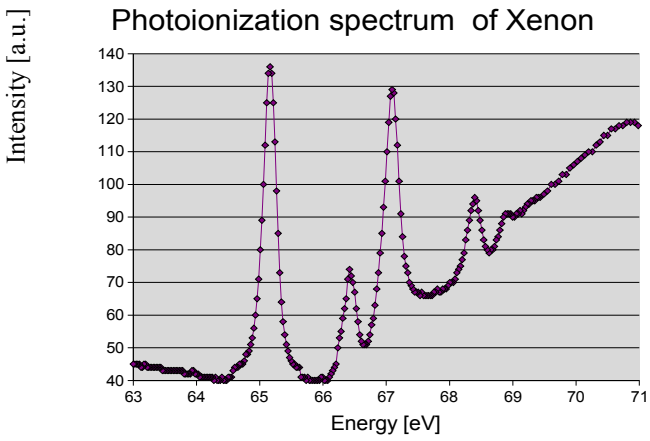

Figure 1: Photoionization spectrum of Xe, measured at BL12, using the $4d_{5/2}$ $4d_{3/2}$ to 6p 7p transition.

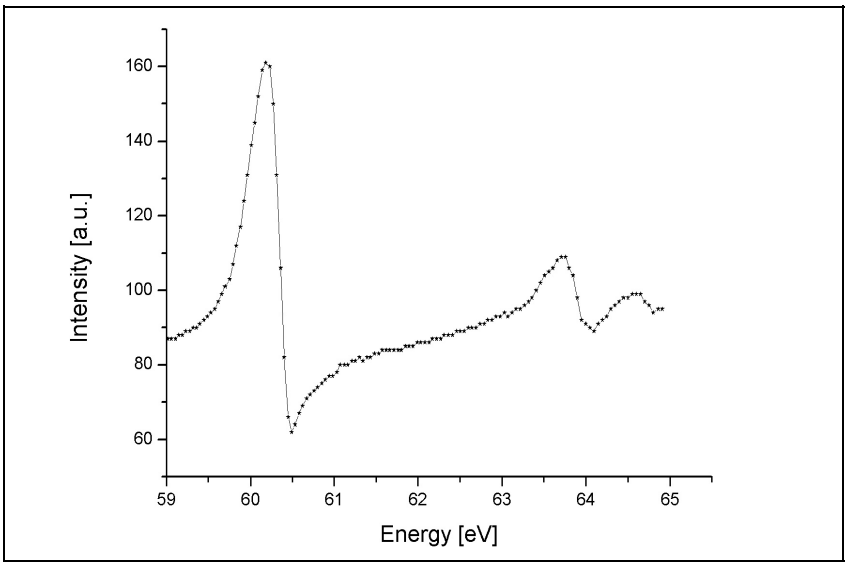

Figure 2: Photoionization spectrum of He, measured at BL12, below the n=2 threshold.

Photoelectron spectroscopy (XPS) studies on the system zirconium oxide on Si(100)

F. Schönbohm[1,2]*, C. Flüchter[1,2], D. Weier[1,2], M. Schürmann[1], U. Berges[1,2], C. Westphal[1,2]

[1] Experimentelle Physik 1 - Universität Dortmund, Otto-Hahn-Str. 4, D 44221 Dortmund, Germany
[2] DELTA - Universität Dortmund, Maria-Goeppert-Mayer-Str. 2, D 44227 Dortmund, Germany
* corresponding author: f.schoenbohm@imail.de

The continuous downscaling in the semiconductor technology during the last decades generates a problem when trying to reduce the gate dielectric thickness below 2 nm. It is well known that SiO_2 gate dielectrics below 2nm lose their effciency because of an increasing leakage current. On the other hand a thinner gate dielectric is desired in order to increase the gate capacity. Therefore a lot of research activities are carried out in order to find alternatives for the presently used SiO_2 gate dielectric. Some promising candidates which could substitute SiO_2 are the so called high-k materials, such as hafnium oxide and zirconium oxide. Because of the importance for industrial manufacturing we studied ultrathin ZrO_2 films on a Si(100) surface. The measurements were performed at the beamline 11 of DELTA. This beamline provides a high energy resolution and a high photon flux at photon energy of $h\nu$ = 320 eV. The sample preparation and the measurements were carried out in a UHV-chamber. The base pressure in the chamber was below $5 \cdot 10^{-11}$ mbar and it rose to approximately $2 \cdot 10^{-10}$ mbar during the evaporation, because of the hot surfaces in the electron-beam evaporator. Clean Si(100) samples in (2x1) reconstruction were used as substrates. On these samples small amounts of ZrO_2 were deposited by electron beam evaporation. During the deposition process, spectra of the Si 2plevel and of the Zr 3d-level were recorded every 15 minutes. Additionally overview spectra were taken in order to check for spurious contaminations. Figure 1 displays photoelectron emission spectra of the sample for an increasing ZrO_2 coverage and for various heat treatments. Part A) shows the decreasing Si 2p intensity due to the damping of the covering ZrO_2 film. In Figure 1 B) the intensity of the Zr 3d signal is plotted. During the evaporation process the ZrO_2 growth rate varied from 0.17 nm and 0.32 nm per evaporation cycle. After 75 minutes of accumulated evaporation the film-thickness of the ZrO_2 deposit shown in the spectra of Figure 1 represents a thickness of approximately 1.1 nm. All prepared samples where annealed in order to study variations of the surface as a function of temperature flash. After a temperature treatment we waited for approximately 40 minutes in order to minimize temperature influences on the peak form and position (Figure 1). Subsequently high resolution XPS spectra of the Si 2p and Zr 3d-levels were recorded. The experimental findings are presented in Figure 1 C) and D). As a result we observe a constant intensity of the Si-2p level for temperatures below 650°C, displayed in Figure 1 C). For annealing temperatures of 650°C and above the intensity of the Si 2p-level grows and reaches its maximum at 725°C and 750°C.

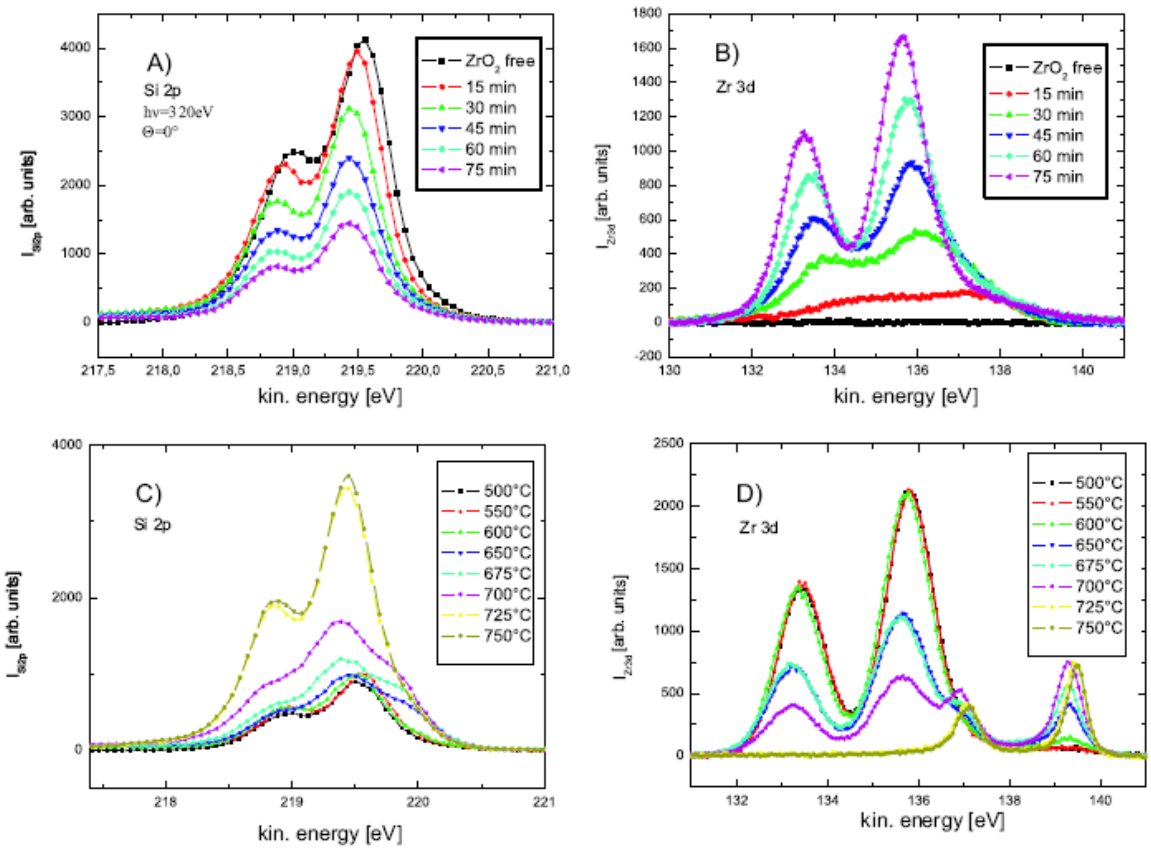

Figure 1: All spectra were taken at $h\nu$ = 320 eV. They were normalized to the DELTA current and a Shirley-Background was substracted. Spectra of the Si 2p-core level during evaporation (A); spectra of the Zr3d-level during evaporation (B), the indicated time refers to the total amount of evaporation; spectra of the Si2p-level during annealing (C); spectra of the Zr3d-level during annealing (D)

Finally, the Si 2p is nearly identical to the signal strength of a clean Si(100) sample. This observation indicates that the former overlaying ZrO_2 film was rearranged due to the heat treatment and small zirconium silicide islands occur at the surface. Therefore clean silicon areas become possible at the surface leading to an increased silicon signal. Also, a broadening of the Si 2p peak for temperatures of 650°C and above indicates the formation of zirconium silicide at the former ZrO_2/Si interface. This finding is also indicated by the spectra of the Zr 3d-level. For a temperature range from 600°C to 700°C the intensity of the ZrO_2 3d level diminishes, as displayed by the spin-orbit-splitted doublet at 133.4 eV and 135.8 eV kinetic energy in Figure 1 D). For temperatures above 600°C a further component rises, which is separated in its kinetic energy by $\Delta E \approx 3.7$ eV to the first component. This new component is due to zirconium silicide formation which was already indicated by the broadening of the Si 2p peak. The lower intensity of the silicide peak compared to the oxide peak is another indication that the sample is covered with zirconium silicide islands.

Acknowledgment

This work was financially supported by the DAAD (No. D-03-23553, Germany), CAPES (Project PROBRAL 170/04, Brazil) and the DFG (We 1649/7-1, Germany). Thanks go to the staff of DELTA for continuous support during the beamtimes.

Depth resolved photoemission experiments with soft x-ray standing waves on multilayer systems

Sven Döring[1,2], Daniel Weier[1,2], Felix Lehmkühler[1,2], Ulf Berges[1,2], F. Salmassi[3], Charles S. Fadley[3,4,5] and Carsten Westphal[1,2]

[1]DELTA, University of Dortmund, Maria-Goeppert-Mayer-Str. 2, Dortmund, Germany
[2]Experimental Physics 1, University of Dortmund, Otto-Hahn-Str. 4, Dortmund, Germany
[3]Materials Sciences Division, Lawrence Berkeley National Laboratory, Berkeley, California USA
[4]University of California, Davis, USA
[5]Forschungszentrum Jülich, Institut für Festkörperphysik, IFF-9, Jülich, Germany

Classical photo-emission using soft x-ray excitation provides a limited depth-resolution, even with the long-standing use of angle-resolved measurements to try to derive nanometer-scale concentration depth profiles. However, for many systems the determination of more accurate depth-profiles, including those involving buried interfaces, is necessary. Sometimes, conventional angle-resolved photo-emission spectroscopy and diffraction may be used for sufficient results, with depth-resolutions limited by the uncertainty of the mean-free path of electrons. Cutting the sample perpendicular to the surface for additional depth profiling via microscopy (e.g. STM or SEM) is not non-destructive and also may lead to ambiguous results if this new surface shows relaxation phenomena.

A newly-developed method for enhancing depth sensitivity in photoemission is to create an oscillatory x-ray standing wave perpendicular to the surface. In the hard x-ray regime, x-ray standing wave techniques are already used to obtain both, Angstrom-scale atomic positions (via Bragg reflection from atomic planes) or concentration depth profiles (via the onset of total reflection for grazing incidence angles). However, the period of the standing wave intensity in the total reflection regime, which is given by $\lambda_{SW} = \lambda_x/2\sin\theta_{inc}$, with λ_x = the x-ray wavelength and θ_{inc} = the x-ray incidence angle, is too high, due to the low incidence angles required, to reach to a depth resolution necessary in many experiments.

Employing standing-wave techniques in the soft x-ray standing wave techniques also leads to some challenges: the reflectivity on most surfaces at non-grazing angle is too low in the soft x-ray regime to provide sufficient standing wave modulations. However, this problem can be solved by using samples incorporation a multilayer mirror. Such multilayers provide a strong first-order Bragg-reflection, according to $\lambda_x = d_{ML}\sin\theta_{inc}$, where d_{ML} is the period of the multilayer. The standing wave field excited at this angle offers a wavelength equal to the period of the multilayer. Thus, a standing wave period based on the multilayer periodicity can be tuned to match to the dimensions of the structures under investigation, which in our case are typically in the nanometer range.

During the simplest type of x-ray standing wave experiment, photoelectron spectra are recorded as a function of the x-ray incidence angle. The intensities of the measured signals are modulated by the standing wave field as a function of the incidence angle. An intensity plot as a function of the incidence angle is called a rocking curve. The modulations of the curve contain information about the thickness and the depth of the layer within the sample, as well as the nature of interface mixing associated with buried layers. For typical multilayers with periods in the range 3-4 nm and consisting of 30-60 bilayers, the rocking curves show their essential part within a degree or less, with this depending on the photon energy and being narrower as the energy is increased. Therefore a high accuracy of the angular movement of the sample must be provided.

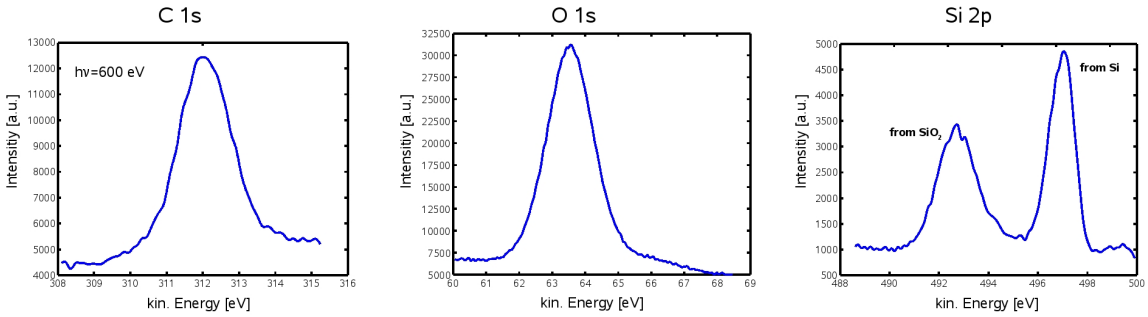

Figure 1: Photoelectron spectra from three core levels in the Si/$MoSi_2$ multilayer sample

An exact knowledge of the electron binding energy is another advantage of the soft x-ray standing wave technique combined with photoemission: Here, the binding energy can be determined with a higher precision compared to more conventional fluorescence detection methods previously used in connection with hard x-ray standing wave measurements. In fact, the binding energy may be determined within a few tenths of an eV in photoemission while the energy resolution is only a few eV in fluorescence measurements. Thus, chemical shifts can be accessed in soft x-ray standing wave photoemission experiments.
A first test of this method at DELTA was carried out in 2007 at the U55 Beamline 11. This beamline provides a high photon flux in the soft x-ray regime at a sufficient energy resolution. The experimental endstation equipped previously for x-ray photoelectron diffraction measurements provides the necessary angular resolution to measure rocking curves on multilayer systems. The measurement of the rocking curves is also fully automated.

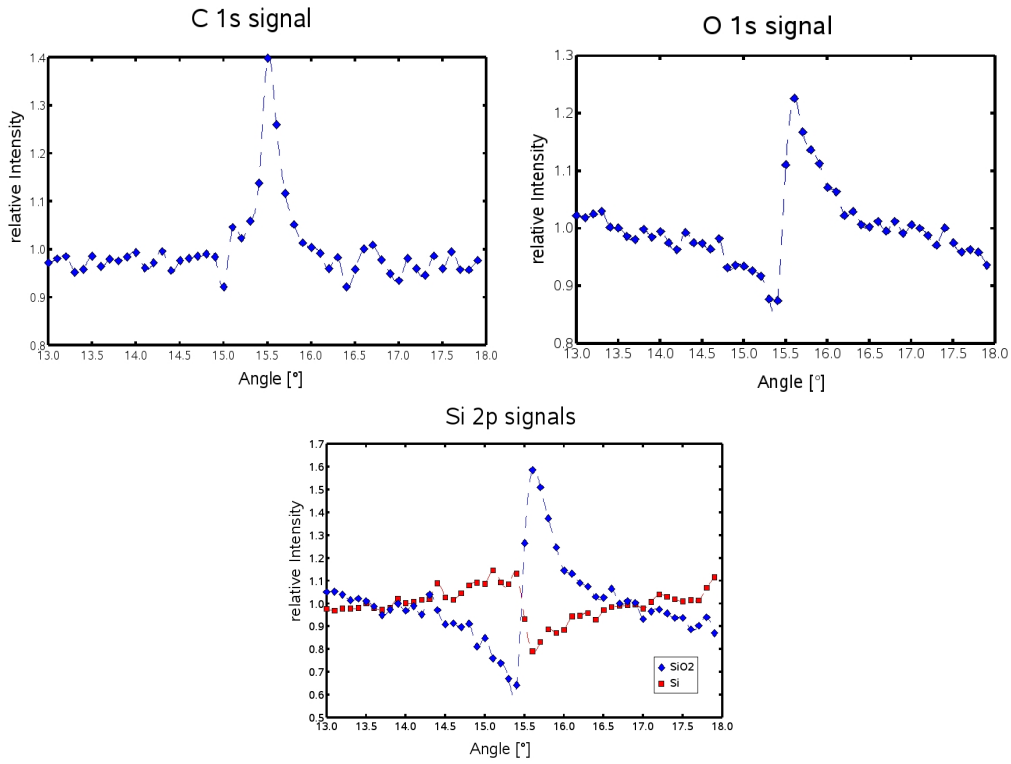

Figure 2: Rocking curves derived from the four resolvable peaks in Fig. 1. The fact that all the curves have very different forms and/or fractional amplitudes is clear evidence of atoms originating in different layers or depths within the sample.

The sample used to explore the possibility of measuring photoemission spectra modulated by a soft x-ray standing wave consisted of a Si/$MoSi_2$ multilayer with 80 double layers, and it was grown in the Center for X-Ray Optics at the Lawrence Berkeley National Laboratory. The silicon- and $MoSi_2$-layers are 28.6 Å and 11.1 Å thick, respectively, as determined by reflectivity measurements with a conventional hard x-ray tube diffraction setup. On top of the sample a thin carbon and oxygen containing contaminant layer was found.
The photoemission signals of carbon 1s, oxygen 1s, and silicon 2p are the most intense signals in the spectrum measured with a photon energy of $h\nu$= 600 eV. Furthermore a chemical shift of 4.2 eV of the silicon 2p signal was observed, permitting the independent measurement of the rocking curves associated with SiO_2 and elemental Si. At a kinetic energy of E_{kin} = 497 eV the photoemission signal of pure silicon was recorded. The chemical shifted signal of silicon, observed at a kinetic energy of E_{kin} = 493, is due to a complete oxidation of silicon.
The incidence angle of the synchrotron light was varied from 13° to 18° angular range with a step size of 0.1°. For each step a set of the three spectra was recorded. Figure 2 shows the photoemission signal of carbon, oxygen, and silicon as a function of the incidence angle.
The quantitative evaluation of the rocking curves is not yet finished, but will make use of a program especially written for this purpose by S.H. Yang at IBM Almaden Research. For the near future more experiments using standing waves are planned. Several different multilayer systems have already been tested for standing wave effects at the DELTA U55 beamline and also at the BESSY HIKE experiment on beamline KMC-1.

Acknowledgement

We would like to thank the DELTA-staff and Physics Department's mechanical workshop for their support. We also thank the staff at LBNL who prepared the sample and the Forschungszentrum Jülich, Institut für Festkörperphysik, IFF-9 group.

Development of a portable wide-energy range micro-focus XRF spectrometer for analysis of aerosol particles from the South Pole

Markus Krämer, Shuji Maeo, Kaori Kuzushita and Kazuo Taniguchi

Osaka Electro-Communication University, 18-8 Hatsucho, Neyagawa, Osaka, Japan.
Fax: +81-72-825-4690; Tel: +81-72-820-4572; E-mail: markus@isc.osakac.ac.jp

Analysis of ice drilling cores from the Antarctic ice cap can deliver vast information about the atmosphere and climatic conditions in the past, depending on drilling depth up to several hundred thousand years back. While the average elemental composition of the atmosphere is represented by the respective concentrations of atoms and ions soluted in the water, respectively ice, dust particles can be probes of sometimes climatically important events such as volcano eruptions or meteorite impacts.

X-ray fluorescence analysis (XRF) is a technique that can be applied well for analyzing these samples. As a wide variety of elements may occur in those dust particles, different photon energies are required for most efficient fluorescence excitation. In addition to that, an energy dispersive fluorescence radiation detection device is necessary to record the fluorescence photons emitted from the sample. Furthermore, it has to be considered that the particles are often smaller than one micrometer, thus it is necessary to provide an X-ray beam of similar dimensions. Finally, samples might have to be characterized in the field requiring a portable device.

In the framework of our project we are developing a portable wide-energy range micro-focus XRF spectrometer according to these demands. A multi-target tube permits switching between Cr, W and Rh targets without the need to open the tube and in such a way covers an energy range between 3 keV and 20 keV. Focusing by an electrostatic lens inside the tube reduces the source size on the target to 10 micrometers.

However, as the beam emitted from an X-ray tube is always divergent it has to be focused to the sample position by some X-ray optical devices. In our project this task is handled by a doubly-curved crystal (DCC) of Si (111). A crystal bended around the beam axis (von Hámos geometry) leads to focusing in direction vertical to the crystal surface (vertical focusing). Additionally, bending the crystal around an axis orthogonal to the direction of the beam (Johann geometry) causes focusing in direction of the beam. Thus, a combination of both permits point-to-point focusing from a micro-source to a micrometer-sized sample.

Instead of Johann geometry the so-called Johansson geometry (with crystal surface and lattice planes having different bending radii) can be applied to achieve exact point-to-point focusing and higher photon intensity at the location of the sample because the reflecting acceptance area of a Johansson crystal is much larger than that of a Johann crystal.

DCCs in Johann geometry have been manufactured in our group by bending thin silicon foils. They provide focal spots of a few tens if micrometers size and photon intensity gains of about three orders of magnitude (relative to a pinhole of the same size). First Johansson crystals bended at high temperatures and milled to the desired shape in a high-precision milling machine are in the testing state by now.

Finally, photon detection is done by an energy dispersive silicon drift detector (SDD). With a peak to background ratio of more than 5000 and - in combination with high tube intensity and focusing efficiency - a low limit of detection is achievable.

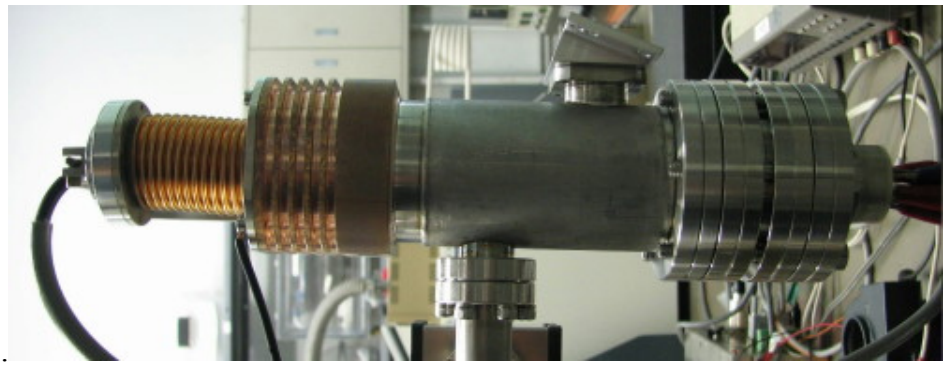

Figure 1: Photo of the microfocus X-ray tube. (Overall length ≈ 30 cm)

Figure 2: Photo of a doubly-curved crystal in Johann geometry. (Size ≈ 25 mm x 30 mm)

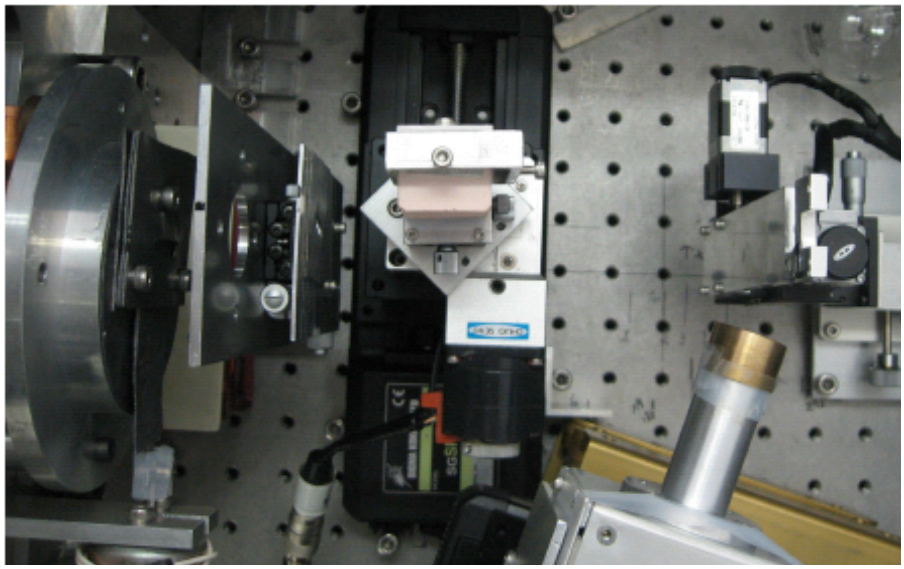

Figure 3: Set-up of tube, entrance slit, DCC, sample and detector.